The FEBS Journal

FEBS PRESS science publishing by scientists

Structural characterisation of nucleotide sugar short-chain dehydrogenases/reductases from the thermophilic pseudomurein-containing methanogen *Methanothermobacter thermautotrophicus* ΔH

Vincenzo Carbone[1], Linley R. Schofield[1], Patrick J. B. Edwards[2], Andrew J. Sutherland-Smith[2] and Ron S. Ronimus[1]

1 AgResearch Ltd., Grasslands, Palmerston North, New Zealand
2 School of Food Technology and Natural Sciences, Massey University, Palmerston North, New Zealand

Keywords
cell wall; dehydratase; epimerase; Methanothermobacter; pseudomurein; SDR

Correspondence
V. Carbone, AgResearch, Grasslands Research Centre, Tennent Drive, Private Bag 11008, Palmerston North 4442, New Zealand
Tel: +64 (06) 351 8331
E-mail: vince.carbone@agresearch.co.nz

(Received 26 February 2025, revised 4 June 2025, accepted 21 August 2025)

doi:10.1111/febs.70248

Epimerases and dehydratases are widely studied members of the extended short-chain dehydrogenase/reductase (SDR) enzyme superfamily and are important in nucleotide sugar conversion and diversification, for example, the interconversion of uridine diphosphate (UDP)-linked glucose and galactose. *Methanothermobacter thermautotrophicus* contains a cluster of genes, the annotations of which indicate involvement in glycan biosynthesis such as that of cell walls or capsular polysaccharides. In particular, genes encoding UDP-glucose 4-epimerase related protein (*Mth375*), UDP-glucose 4-epimerase homologue (*Mth380*) and dTDP-glucose 4,6-dehydratase related protein (*Mth373*) may be involved in the biosynthesis of an unusual aminosugar in pseudomurein. In this paper, we present the structures of Mth375, an archaeal sugar epimerase/dehydratase protein (WbmF) determined to a resolution of 2.0 Å. The structure contains an N-terminal Rossmann-fold domain with bound nicotinamide adenine dinucleotide hydride (NADH) and a C-terminal catalytic domain with bound UDP. We also present the structure for Mth373 co-crystallised with uridine-5′-diphosphate-xylopyranose to a resolution of 1.96 Å as a NAD^+-dependent oxidative decarboxylase (UDP-xylose synthase; EC4.1.1.35). Molecular modelling has also allowed for the identification of Mth380 as a UDP-*N*-acetylglucosamine 4-epimerase (WbpP; EC5.1.3.7), Mth631 as a UDP-glucose 4-epimerase (GalE; EC5.1.3.2) and Mth1789 as a classical dTDP-D-glucose 4,6-dehydratase (EC4.2.1.46). The UDP–sugar specificity of each archaeal nucleotide sugar short-chain dehydrogenase/reductase

Abbreviations
AMP, adenosine 5′-monophosphate; CEP1, carbohydrate epimerase family 1; CME, S,S-(2-hydroxyethyl)thiocysteine; Da, Dalton; DAU, 2′deoxy-thymidine-5′-diphospho- α-D-glucose; DNA, deoxyribonucleic acid; dTDP, thymidine diphosphate; dTGD, dTDP-glucose 4,6-dehydratase; DTT, dithiothreitol; EPZ, UDP-*N*-acetyl-α-D-muramic acid; EX-L, extended loops; GDP, guanosine diphosphate; Glc, glucose; GlcN, glucosamine; GlcNAc, *N*-acetylglucosamine; GOL, glycerol; HEPES, 2-[4-(2-hydroxyethyl)piperazin-1-yl]ethanesulfonic acid; HP7, UDP-*N*-acetyl-D-glucosaminuronate; LPS, lipopolysaccharide; MOPS, 3-(*N*-morpholino)propanesulfonic acid; Mth, *Methanothermobacter thermautotrophicus* ΔH; NAcTalNA, *N*-acetyltalosaminuronic acid; NADH, nicotinamide adenine dinucleotide hydride; NAT, *N*-acetyl-L-talosaminuronic; NCBI, National Center for Biotechnology Information; NS-SDR, nucleotide sugar short-chain dehydrogenases/reductases; PDB, Protein Data Bank; PEG, polyethylene glycol; PMSF, phenylmethylsulfonyl fluoride; RCSB, Research Collaboratory for Structural Bioinformatics; RMSD, root mean square deviation; SDR, short-chain dehydrogenase/reductase; SDS/PAGE, sodium dodecyl sulfate polyacrylamide gel electrophoresis; TCEP, tris (2-carboxyethyl) phosphine; TM, transmembrane); Tris, tris (hydroxymethyl)aminomethane; TYD, thymidine-5′-diphosphate; UAXS, UDP-D-apiose/UDP-D-xylose synthase; UD1, UDP-*N*-acetylglucosamine; UDP, uridine-5′-diphosphate; UDP-GlcNAc, UDP-*N*-acetylglucosamine; UDX, UDP-xylopyranose; UGA, UDP-glucuronic acid; UPG, UDP-glucose; UXS, UDP-α-D-xylose synthase.

(NS-SDR) was elucidated via sequence, molecular modelling and structural analyses. Overall, these structures potentially shed light on the formation of the glycan portion of pseudomurein and capsular polysaccharide in Archaea.

Introduction

Cell walls are important for the survival of prokaryotes by enabling the preservation of cell shape from osmotic stresses [1–4]. Almost all bacteria contain peptidoglycan (murein) in their cell walls, the biosynthesis of which has been extensively investigated [5–8], while archaea possess an array of cell walls none of which are closely related to peptidoglycan [2,9]. These include methanochondroitin, sulfated heteropolysaccharides, S-layers, proteinaceous sheaths, glutaminylglycans, halomucin, polysaccharide-based glycocalyces or pseudomurein, depending on their phylogenetic affiliation [2,9–14]. The latter cell wall type, pseudomurein, is found in the orders Methanobacteriales and Methanopyrales and at a very basic component level, is analogous to peptidoglycan in that it contains both a glycan backbone and a peptide cross-link [15–17]. However, the amino sugars in the glycan backbone are linked through β(1–3) bonds, the peptide cross-link only contains L-amino acids and the pentapeptide incorporates several isopeptide bonds [10,16,17]. In addition, pseudomurein universally contains an unusual amino sugar moiety, *N*-acetyl-L-talosaminuronic (NAT) acid which typically alternates with either *N*-acetylglucosamine or *N*-acetylgalactosamine residues (Fig. 1) [15–19]. Neutral nonacetylated sugar residues glucose (Glc) and glucosamine (GlcN) can also be present. The presence of *N*-acetylglucosamine or *N*-acetylgalactosamine residues varies dependent on species [10]; for *Methanothermobacter thermautotrophicus* ΔH, *N*-acetylglucosamine residues predominate [10]. The overall differences in chemistry and biosynthesis between pseudomurein and peptidoglycan are large enough that it has been hypothesised that the two cell wall types are likely to have evolved independently [2,16,17], though the bacterial Mur and archaeal pMur peptide ligases share a common evolutionary history [20,21].

The biosynthesis of the unusual *N*-acetyl-L-talosaminuronic acid in pseudomurein is hypothesised to be achieved by epimerisation and oxidation of UDP-*N*-acetylgalactosamine. Methanobacterial and *Methanopyrus kandleri* genomes contain easily identifiable orthologues of bacterial GlmS (glucosamine-fructose-6-phosphate aminotransferase; EC2.6.1.16), GlmM (phosphoglucosamine mutase; EC5.4.2.10) and the bifunctional GlmU (bifunctional UDP-*N*-acetylglucosamine pyrophosphorylase/glucosamine-1-phosphate *N*-acetyltransferase; EC2.7.7.23 and EC2.3.1.157). These enzymes have the capability to produce UDP-*N*-acetylglucosamine, an amino sugar residue in the glycan backbone of most pseudomurein-containing methanogens [10,11,16,17,22,23]. In addition, most of these genomes also contain at least one annotated UDP-*N*-acetylglucosamine 2-epimerase (WecB; EC5.1.3.14) and all contain at least one UDP-glucose 4-epimerase (GalE; EC5.1.3.2 [22]), although both of these epimerase types have not yet been functionally characterised from any methanobacterium or *Methanopyrus kandleri* strain [24,25]. In recent efforts, we have structurally characterised a WbpP (UDP-*N*-acetylglucosamine 4-epimerase; EC5.1.3.7) from *Methanobrevibacter ruminantium* [26].

Van Overtveldt *et al.* [27] reviewed carbohydrate epimerases and classified them based on reaction mechanisms and structure. The CEP1 family (carbohydrate epimerase family 1) includes both UDP-glucose 4-epimerases (EC5.1.3.2) and GDP-mannose 3,5-epimerases (EC5.1.3.18) with the same reaction mechanism [27]. This suggests that *M. thermautotrophicus* UDP-glucose 4-epimerase orthologues could potentially encode enzymes that are capable of 3,5-epimerisation. Interestingly, protein sequence searches indicate that *M. thermautotrophicus* ΔH potentially possesses several enzymes with UDP-glucose 4-epimerase activity (Mth373, Mth375, Mth380, Mth631 and Mth1789) [22,28]. These enzymes are found in a large gene cluster in *M. thermautotrophicus* suggestive of a role in either cell wall biosynthesis or capsular polysaccharide formation [20,21,28], and with Mth375 and Mth380 annotated as UDP-glucose 4-epimerase-related enzymes, and Mth373 annotated as a dTDP-glucose 4,6-dehydratase (dTGD) related protein. Additional enzymes of note within this gene cluster include Mth370 a LPS biosynthesis RfbU-related protein, Mth371 a glycosyltransferase RgtA/B/C/D-like domain-containing protein, Mth374 a dolichyl-phosphate mannose synthase-related protein, Mth376

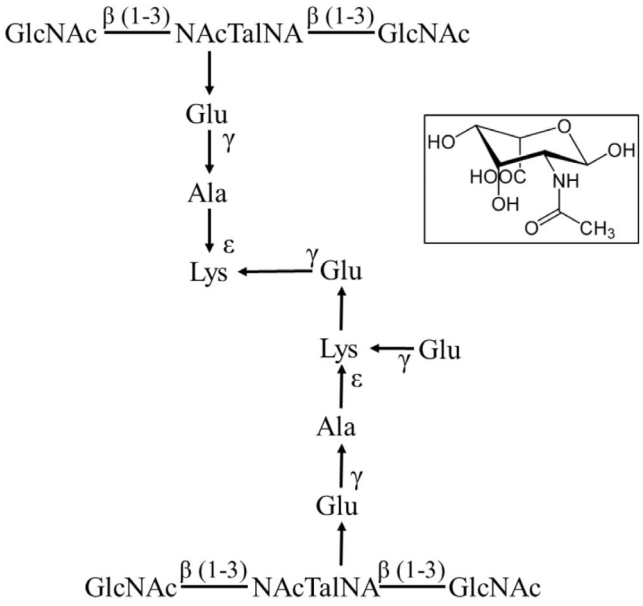

Fig. 1. Methanogen pseudomurein. Methanogen pseudomurein contains amino sugars in the glycan backbone linked through β (1–3) bonds, the unusual amino sugar NAcTalNA, L-amino acids and several unusual isopeptide bonds. Inset: The structure of NAcTalNA. The figure was adapted and modified from Schofield *et al.* [77]. GlcNAc, *N*-acetylglucosamine; NAcTalNA, *N*-acetyltalosaminuronic acid.

a glycosyl transferase-related protein, Mth377 a dolichyl-phosphate mannose synthase-related protein, Mth378 a lysylphosphatidylglycerol synthase TM region and Mth379 an *O*-antigen transporter-related enzyme.

To gain a better understanding of *N*-acetyl-L-talosaminuronic acid synthesis and more generally aminosugar conversions in pseudomurein-containing methanogens, we have chosen to investigate NS-SDRs from the model species *Methanothermobacter thermautotrophicus* ΔH for structural studies. In this paper, we present two structures of Mth375, an archaeal sugar epimerase/dehydratase (WbmF; with UDP bound) and two structures of Mth373, a NAD^+-dependent oxidative UDP-glucuronic acid decarboxylase (EC 4.1.1.35; with UDX bound). The enzyme structures revealed that Mth375 has a similar fold and active site to bacterial GalE 4-epimerases (EC5.1.3.2), UDP-glucuronate decarboxylases (EC4.1.1.35), WbpP, and WbgU (EC5.1.3.7) enzymes, while Mth373 shares conserved protein domains with the NAD^+-dependent epimerase/dehydratase family of proteins, including WcaG [29,30] placing both enzymes within the SDR superfamily. Molecular modelling and sequence alignment enabled the functional prediction of Mth380 as a WbpP (EC5.1.3.7), Mth631 as another GalE 4-epimerase (EC5.1.3.2) and Mth1789 as a classical dTGD (EC4.2.1.46).

Results and discussion

Crystal structure of Mth375

Mth375 expressed with high yield in culture and did not require further purification after nickel-affinity chromatography, eluting as a single peak with SDS/PAGE analysis showing a purity in excess of 95%, appropriate for protein crystallisation. Mth375_AU crystallised in the trigonal space group *H 32* with unit cell parameters a = 113.8 Å, b = 113.8 Å, c = 239.9 Å, α = 90.0°, β = 90.0° and γ = 120.0°. There was a single monomer in the asymmetric unit (Fig. 2A) with a solvent content estimated to occupy 65% of the unit cell volume and a Matthews coefficient of 3.51 $Å^3 \cdot Da^{-1}$. Mth375_NU crystallised in the hexagonal space group *P 6₃ 2 2* with unit cell parameters a = 89.3 Å, b = 89.3 Å, c = 174.7 Å, α = 90.0°, β = 90.0° and γ = 120.0° and contained one monomer in the asymmetric unit, with a solvent content occupying 47% of the unit cell volume and a Matthews coefficient of 2.32 $Å^3 \cdot Da^{-1}$ (see Table 1 for all refinement and geometric statistics). After structure determination and refinement, the electron density for both Mth375 complexes was consistent throughout the structures and was unbroken for the main chain of 332 residues, but with a few instances of side chain disorder at the N terminus. Both crystal structures present a single

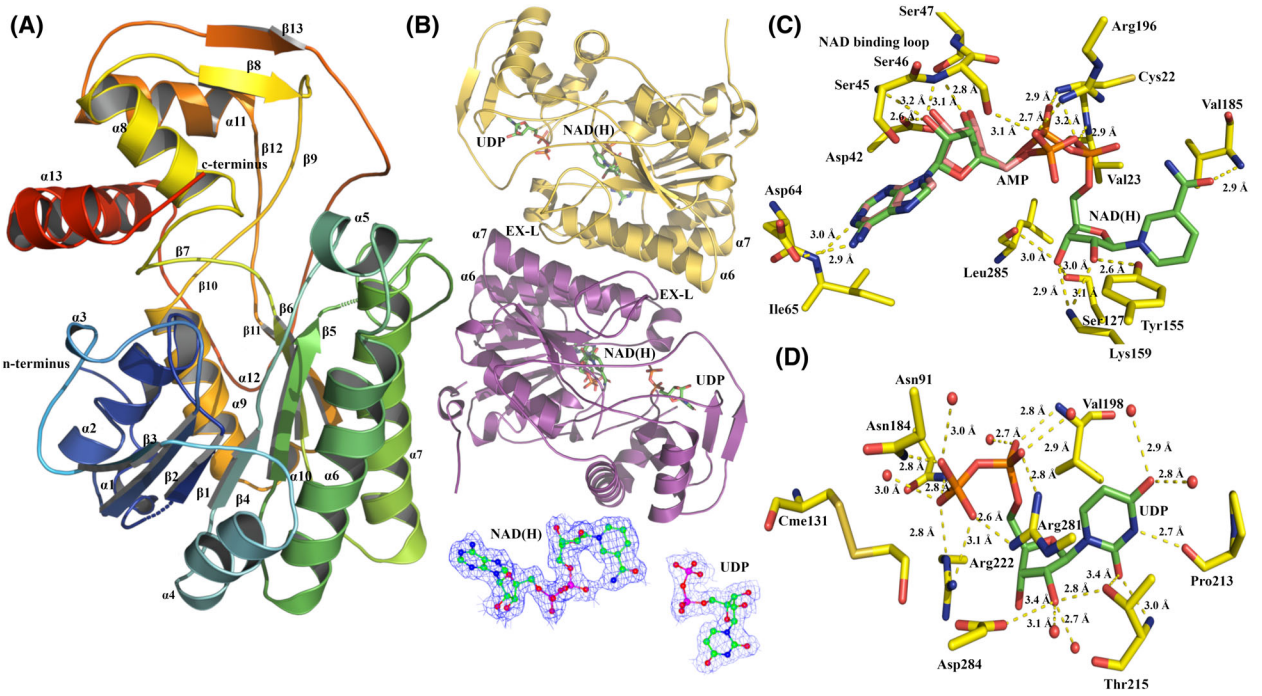

Fig. 2. Structures of *M. thermautotrophicus* ΔH Mth375. (A) A ribbon representation of Mth375 (WbmF; nucleotide sugar epimerase/dehydratase) with secondary structural elements labelled. The structure is colour-ramped from the N terminus (blue) to C terminus (red). (B) Dimeric Mth375_NU with bound molecules, helices α_6 and α_7 and the extended loop labelled (EX-L). Immediately below depicts the 2Fo-Fc electron density maps of the refined NADH and UDP molecules. (C) The coenzyme-binding domain of Mth375_NU depicting NAD(H) (carbons in green) and the superimposed AMP molecule bound to Mth375_AU (carbons in pink). (D) The Mth375_NU active site domain with bound UDP (carbons are coloured green). Relevant residues and water molecules are shown (by atom; Mth375 carbons are in yellow). All polar contacts and distances are indicated with dashed lines. All figures were prepared using PyMOL version 2.5.8.

modified active site cysteine (Cys131), while Mth375_NU has a second modified cysteine (Cys13) derivatised by β-mercaptoethanol present in the storage buffer to form *S*,*S*-(2-hydroxyethyl)thiocysteine (CME). In Mth375_AU a single molecule of adenosine 5′-monophosphate (AMP) was detected in the N-terminal coenzyme-binding domain and a single molecule of UDP in the Mth375 active site. The presence of AMP was a consequence of crystallisation with Silver Bullets Bio screen condition containing 0.20% (w/v) of AMP sodium salt. Mth375_NU contained a single NADH molecule, and like Mth375_AU, a single molecule of UDP was present in the active site of the enzyme. *N*-acetyl-D-glucosamine added to the mother liquor prior to freezing Mth375_NU crystals failed to bind in the crystal structure. For both complexes, the UDP molecules superimpose in an identical manner as do the adenosine moieties of AMP and NADH.

The Mth375 monomer contains two distinct structural domains and common sequence characteristics that are widespread amongst the SDR enzyme superfamily (Fig. 2A,B) [31,32]. The domains are an N-terminal nucleotide-binding domain (residues 1–183) predominantly formed by a modified Rossmann-fold motif which in Mth375 binds NADH and a C-terminal active site domain (residues 184–332) that binds the UDP-sugar substrate. This fold is common amongst archaeal, bacterial and eukaryotic 4-epimerases [24,26,33], a family of enzymes denoted either as GalE (EC 5.1.3.2; UDP-glucose/galactose 4-epimerases), WbpP or WbgU (EC 5.1.3.7; UDP-*N*-acetylglucosamine/galactosamine 4-epimerases). The N-terminal coenzyme-binding domain incorporates a series of seven parallel β-strands (residues 14–18 β_1, 37–42 β_2, 57–63 β_3, 80–85 β_4, 123–130 β_5, 176–183 β_6 and the C-terminal residues 246–250 β_{11}) and ten α-helices (residues 1–10 α_1, 22–34 α_2, 49–51 α_3, 67–76 α_4, 90–97 α_5, 98–120 α_6, 153–174 α_7 and the C-terminal residues 227–239 α_9, 241–244 α_{10} and 293–301 α_{12}). The parallel β-strands are sandwiched on one side by α-helices α_1, α_2, α_3, α_9, α_{10} and α_{12} and on the other by α-helices α_4, α_5, α_6 and α_7. The characteristic SDR superfamily [24,31,32,34] extended coenzyme-binding motif ***G*-*X*-*X*-*G*-*X*-*X*-*G*** is located on the short loop

Table 1. Data collection and refinement statistics.

	Mth375_AU AMP & UDP Mth375	*Mth375_NU NAD & UDP Mth375*	*Mth373_NU NAD & UDP Mth373*	*Mth373_NX NAD & UDX Mth373*
PDB code	6PMH	6PNL	8W3U	9AR1
Space group	H 3 2	P 63 2 2	P 2 2 21	H 3 2
Unit cell parameters				
a, b, c (Å)	113.8, 113.8, 239.9	89.3, 89.3, 174.7	54.5, 81.4, 152.4	139.3, 139.3, 226.9
α, β, γ (°)	90.0, 90.0, 120.0	90.0, 90.0, 120.0	90.0, 90.0, 90.0	90.0, 90.0, 120.0
Wavelength (Å)	0.91170	0.95364	0.95370	0.95368
Temperature (K)	100	100	100	100
Resolution Range (Å)	48.27–2.30	46.5–2.01	45.27–2.00	44.71–1.96
No. of observed ref.[a]	298 565 (29548)	540 821 (36612)	672 781 (29403)	1 186 053 (60087)
No. of unique ref.[a]	26 918 (2607)	28 060 (1958)	48 712 (2617)	59 615 (3405)
R_{sym}[a]	0.176 (0.763)	0.182 (0.932)	0.192 (0.768)	0.162 (0.615)
R_{pim}[a]	0.055 (0.237)	0.043 (0.216)	0.076 (0.304)	0.037 (0.145)
Completeness (%)[a]	100.0 (100.0)	99.7 (96.3)	99.8 (98.0)	98.6 (80.6)
Multiplicity[a]	11.1 (11.3)	19.3 (18.7)	7.3 (7.2)	19.9 (17.6)
I/σ(I)[a]	15.1 (3.7)	16.1 (4.6)	9.4 (2.7)	16.3 (5.3)
CC(1/2)	0.996 (0.905)	0.996 (0.867)	0.994 (0.796)	0.996 (0.951)
Refinement statistics				
Resolution range (Å)	91.17–2.3	87.35–2.01	81.38–1.99	106.5–1.97
All reflections used	26 926	28 075	46 881	60 315
Size R free set (%)	5	5	5	5
All reflections (R free)	1380	1382	2290	2999
R factor (%)	14.71	16.19	16.35	17.24
R free (%)	17.76	18.95	20.39	20.51
Matthews coefficient ($Å^3 \cdot Da^{-1}$)	3.51	2.32	2.29	3.03
Solvent content (%)	64.7	46.5	46.3	59.4
RMSD Bond Length (Å)	0.012	0.0083	0.011	0.11
RMSD Bond Angle (°)	1.61	1.40	1.53	1.64
Ramachandran plot				
Residues in favoured regions (%)	94.1	93.1	91.1	91.1
Residues in allowed regions (%)	5.9	6.9	8.9	8.9
Average B factors ($Å^2$)				
Protein	25.6	22.2	16.5	27.8
UDP	22.5	21.9	14.0	39.2
AMP	17.1	–	–	17.9
NAD	–	16.2	12.3	22.2
UDX	–	–	–	
Ethylene glycol	–	42.7	27.5	38.2
Water	31.3	31.3	23.6	34.7
SO_4^{2-}	–	65.2	–	–
Glycerol	35.2	–	–	38.9
Cl^-	60.4	–	30.9	–
PO_4^{3-}	28.3	–	–	–
Mg^{2+}	–	–	21.6	–

[a]Data in the highest resolution shell are given in parentheses.

between β_1 and α_2 (Fig. 2C; coenzyme loop 1; residues 18–24) with sequence ***G*-*G*-*A*-*G*-*C*-*V*-*G***. Three additional loops make contact with the bound NADH including residues 43-48 (coenzyme loop 2) between β_2 and α_3, residues 63-66 (coenzyme loop 3) between β_3 and α_4 and residues 86–90 (coenzyme loop 4) between β_4 and α_5. An extended loop (residues 130–153) also straddles both the substrate and coenzyme-binding domains between β_5 and α_7. The smaller Mth375 C-terminal domain is comprised of six short β-strands (formed by residues 184–186 β_7, 212–216 β_8, 220–222 β_9, 225–226 β_{10}, 256–257 β_{12} and 274–278 β_{13}) and three large α-helices (formed by residues 197–207 α_8, 258–269 α_{11} and 308–329 α_{13}). A catalytic motif

common amongst SDRs (***Y***-*X*-*X*-*X*-***K***) [24,31] is located on α_7, with sequence ***Y***-*Q*-*V*-*T*-***K*** (residues 155–159). Interactions with UDP and Mth375 are depicted in Fig. 2D and are maintained in part by secondary structure elements α_7, α_8, β_7, β_8, β_9, α_{11} and α_5, and the active site loop between β_9 and α_{12}.

Mth375 is a dimer (Fig. 2B) with a total buried surface of 6689 Å^2 and a dissociation complex ΔG^o_{diss} of 12.4 kcal·mol^{-1} as calculated by PISA [35]. The dimeric structure is maintained via hydrogen bonds between residues present on the adjacent extended loops (EX-L) between β_5 and α_7 which stack along opposing helices (α_7). This includes the side chain of Asn167 (ND2) and the main chain carbonyl of Ile149 (O; 2.9 Å), and the side chain of Asn171 (ND2) which forms hydrogen bonds to the main chain of Leu151 (O; 3.0 Å) and the side chain of Ser150 (OG; 2.9 Å). We also observe identical secondary structure elements α_6 and α_7 from each monomer stacking along each other in an antiparallel fashion where multiple hydrophobic contacts are made forming a singular water-excluding patch predominantly between Leu102, Leu107, Ile109, Leu110, Leu113, Val157, Leu160, Leu161, Leu164, Tyr165, Tyr168 and Phe169.

Mth375_NU revealed interpretable density for the molecule NAD(H). Its presence was not unexpected and is consistent with the conservation of coenzyme binding within epimerases such as GalE [33] by the NAD(H)-binding loop (residues 43–48 in Mth375) forming interactions with the adenine and ribose moiety of NAD(H) (Fig. 2C). The competitive exclusion of the NAD(H) coenzyme by AMP in Mth375_AU is understandable as both molecules form equivalent interactions with the enzyme with their equivalent moieties. The conserved coenzyme-binding motif (sequence ***G***-*G*-*A*-***G***-*C*-*V*-***G***) makes hydrogen bond contacts with the pyrophosphate bridge of NADH and main chain amines of Cys22 (N) and Val23 (N). The NAD(H)-binding loop forms numerous hydrogen bond contacts with the NAD(H) ribose sugar including the side chain carboxylate of Asp42 (OD1), the side chain of Ser47 (OG), and with the main chain of Ser45 (N) and Ser46 (N). The side chain of Ser46 also makes an additional contact with the pyrophosphate bridge (OG) as does the side chain of Arg196 (NH1). The adenine moiety forms hydrogen bond contacts with the Ile64 main chain (N) and side chain of Asp64 (OD1) while the remaining bonds are between the ribosylnicotinamide moiety of NAD(H) and residues Ser127 (OG), Leu85 (O), Lys159 (NZ), Tyr155 (OH) and Val185 (N).

A single molecule of UDP was bound to each Mth375 complex (Fig. 2D). The UDP diphosphate moiety forms a number of hydrogen bond interactions with Asn91 (ND2), Asn184 (ND2), Arg222 (NE and NH2), Arg281 (NH1 and NH2) and Val198 (N), and water molecules including O98, O29, O109 and O146. The UDP ribose hydroxyls form hydrogen bond contacts with the side chain and main chain of Thr215 (OG1 and O) and water molecules O33, O135 and O52. The carbonyl groups present on the uracil moiety make hydrogen bond interactions with waters O64 and O141, the side chain hydroxyl and main chain of Thr215 (OG1 and N), while the 2′-amide forms a hydrogen bond with Pro213 (O).

Probing the sugar-binding domain of Mth375

Some epimerases possess a larger active site to incorporate and rotate an acetylated saccharide moiety during catalysis, which is not the case for the smaller UDP-galactose/glucose substrates of GalE. When comparing the signature key residues of WbpP from *P. aeruginosa* (PDB: 1SB8; Gly102, Ser103, Val104, Tyr166, Asn195, Ala 209 and Ser306) [36] with Mth375, significant differences arise. The corresponding residues in Mth375 include Phe89, Ala90, Asn91, Tyr155, Asn184, Asn197 and Leu289. Significant clashes would likely occur between the UDP-GlcNAc acetyl group during 4-epimerisation with the sidechains including Leu289, Phe89, Asn91, Asn197 and Cys131. ConSurf analysis of the sugar-binding domain indicates that these residues are the most variable in the active site (see Fig. 3A) and often the most common amino acid has a smaller sidechain. Overall, 4-epimerisation of an acetylated sugar is unlikely to occur for Mth375.

When comparing GalE enzymes such as those from *Burkholderia pseudomallei* (PDB: 3ENK) the bound UPG molecule makes several interactions with key

Fig. 3. The substrate binding domain of Mth375. (A) ConSurf depiction and analysis of Mth375 sugar-binding domains [73]. The table details the top amino acids in terms of % conservation (matching residues are coloured red) for each position. (B) Clustal Omega (0.1.2.4) [38] sequence alignment of WbmF enzymes Mth375 (accession number O26475) and PDB: 2Q1S (*Bordetella bronchiseptica*; accession number O87989). Active site residues within 5 Å of the bound substrate are coloured yellow, '*' indicates identical residues, ':' and '.' indicate sequence similarity. (C) Potential substrates docked into the Mth375 crystal structure, including HP7 (carbon atoms coloured yellow), UPG (blue), UGA (green) and UD1 (pink). Compounds were docked using GOLD [39] with the top ranked poses for each compound depicted. Structure figures were prepared using PyMOL version 2.5.8.

Amino Acid	% occurrence of amino acids in the equivalent position		
F89	G 31.1	V 16.9	P 13.5
A90	S 59.7	G 17.5	A 10.7
N91	V 73.2	N 17.5	I 4.7
S129	S 90	A 5.3	T 4
G130	G 95.7	A 4.4	
C131	S 66	C 16.7	A 12
Y155	Y 100		
K159	K 99.3		
N184	N 90.7	T 6	S 1.3
N197	A 48	N 18	G 16
L289	S 59.6	T 15.4	L 11

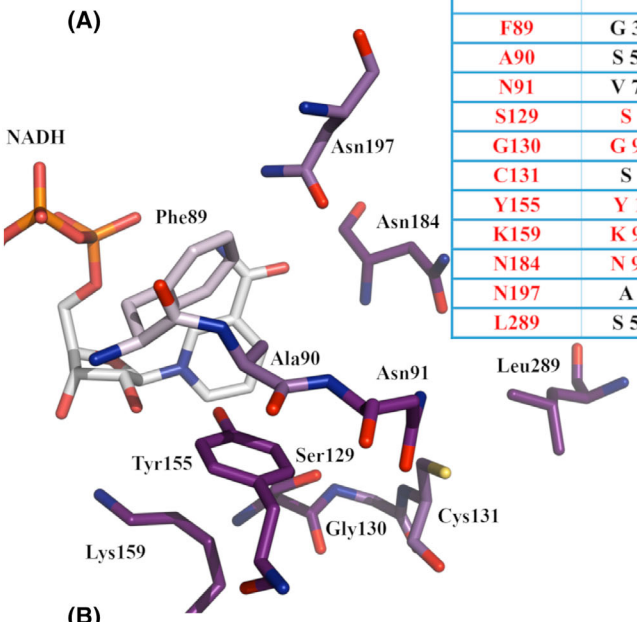

(B)

```
MTH375          --MIMDEFRAYDGKCVLVTGGAGCVGSNLTGNLAKAGAN-VIILDNLSSSYEWNIPEYEN 57
2Q1S (WbmF)     MPVIMN-ASKLANTNVMVVGGAGFVGSNLVKRLLELGVNQVHVVDNLLSAEKINVPDHPA 59
                  :**:       .. *:*.**** *****. .* : *.* * ::*** *: : *:*::

MTH375          IEFVKGDILDDEVLKRVFKERPDYVFHLAAHFANQNSVDNPEKDLLVNGLGILKVLEY-A 116
2Q1S (WbmF)     VRFSETSITDDALLA-SLQDEYDYVFHLATYHGNQSSIHDPLADHENNTLTTLKLYERLK 118
                :.* : .* ** :*   :::. *******:::.**.*:.:*  *   * *  **: *

MTH375          QLVGVERFVYSSSGCGVYGLDS--KIPFEEHDIS--ISLHTPYQVTKLLGELYTNYFHNL 172
2Q1S (WbmF)     HFKRLKKVVYSAAGCSIAEKTFDDAKATEETDIVSLHNNDSPYSMSKIFGEFYSVYYHKQ 178
                ::  :::.***::**.:           ** **    . .:**.::*::**:*: *:*:

MTH375          YEMPIVNARFFNVFGPGEVPG----------KYRNVIPNFFYWAMNQQPLPITGDGSETR 222
2Q1S (WbmF)     HQLPTVRARFQNVYGPGEILGAGRWRGTPATVWRNVTPTFIYKALKGMPLPLENGGVATR 238
                :::* *.*** **:****: *           :*** *.*:* *::  ***: ..*  **

MTH375|         DWTFVEDIVRGLMAMGVRREAIGEAINLGSGTEHQVIEMAGIINELTENPAGVVYRPRRD 282
2Q1S (WbmF)     DFIFVEDVANGLIACAADG-TPGGVYNIASGKETSIADLATKINEITGNNTELDRLPKRP 297
                *: ****:..**:* ..   : * . *:.**.* .: ::*  ***:* * : :   *:*

MTH375|         WDAKTRLLSSIDKARRLLDYEPQVSFREGLERTHRWFTENWELIRKSAEF---------- 332
2Q1S (WbmF)     WDNSGKRFGSPEKARRELGFSADVSIDDGLRKTIEWTKANLAVIEQIMRKHDSALATYGK 357
                ** . : :.* :**** *.:. :**: :**.:* .* . *  :*.:  .
```

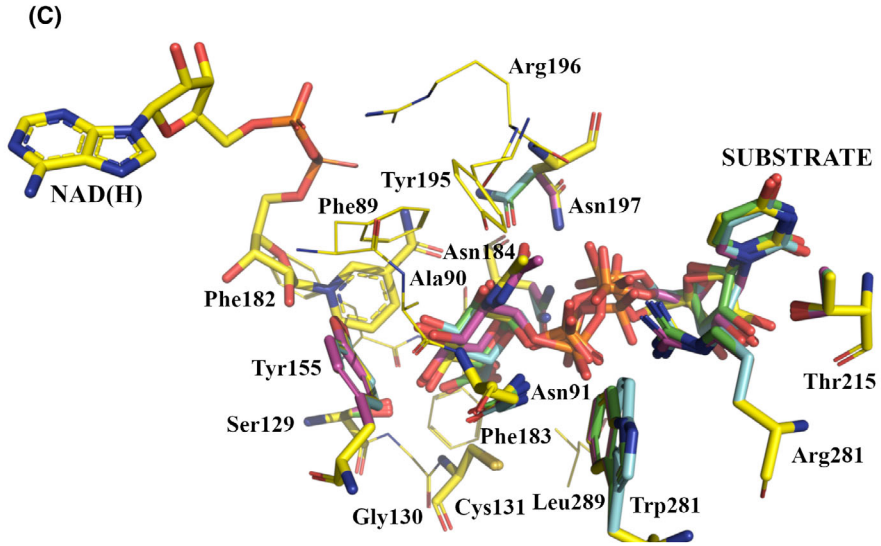

active site residues including Lys88, Ala89, Val90, Tyr152, Asn182, Asn202 and Cys302, which is dissimilar to the architecture of Mth375 (Phe89, Ala90, Asn91, Tyr155, Asn184, Asn197 and Leu289). Structural alignment of both enzymes shows that the hydroxyl groups of UPG do form several potential hydrogen bond contacts with multiple Mth375 residues; however, an observed steric clash with Asn91 would require a large rotameric movement of the sidechain to allow the 4-epimerisation reaction mechanism to proceed.

The pliable active site architecture of this enzyme group explains why Mth375 shares structural homology with multiple epimerase classes shown in Table 2, where a topology-based assessment of Mth375_NU using CLICK [37] was undertaken. The structural homologues of Mth375 included the bacterial 4-epimerase subfamilies known as WbgU (PDB: 3RUF; EC5.1.3.7), GalE (PDB: 2P5Y and PDB: 3KO8; EC5.1.3.2), human UDP-glucuronate decarboxylase (PDB: 2B69; EC4.1.1.35), bacterial WbpP (PDB: 1SB8; [36]), bacterial NAD-dependent epimerase/dehydratase (PDB: 3VPS; EC 4.2.1) and a likely 3,5-epimerase WbmF belonging to the pathogenic bacteria *Bordetella bronchiseptica* (PDB: 2Q1S and PDB: 2PZJ; [34]). Sequences of selected structures from Table 2, with varying activities, were submitted to the Clustal Omega (0.1.2.4) alignment server [38] and residues within 5 Å of the Mth375 UDP molecule were highlighted. The highest active site and overall sequence identity is with *Bordetella bronchiseptica* WbmF (PDB: 2Q1S; Fig. 3B, Table 2) which clades in Group 3 (PDB: 2PZJ; Fig. 4). Enzymes in this class present a strong preference for an acetylated substrate, for example, *B. bronchiseptica* WbmF catalyses the 3,5-epimerisation required in the conversion of UDP-2,3-diacetamido-2,3-dideoxy-D-mannuronic acid to UDP-2,3-diacetamido-2,3-dideoxy-L-galacturonic acid [34]. Furthermore, a sequence and structural comparison of the potential sugar-binding residues of Mth375 with UDP bound WbmF (PDB: 2Q1S) and GalE bound to UPG (PDB: 3ENK) reveals the following active site Mth375/WbmF/GalE fingerprints: Phe89/His90/Lys88, Ala90/Gly91/Ala89, Asn91/Asn92/Val90, Ser129/Ala131/Ser128, Cys131/Cys133/Thr130, Tyr155/Tyr161/Tyr152, Asn184/Asn190/Asn182, Asn197/Asn213/Asn202, Arg281/Arg296/Arg295 and Trp283/Trp298/Gly297. WbmF enzymes have a conserved catalytic cysteine (Cys133) in an identical position as the modified cysteine of Mth375 (Cys131); however, it is structurally disordered in the WbmF crystal structure as are residues Ser134-Thr146. This disorder may be the reason for the large deviation in secondary structure elements around the active site of WbmF and the reason we observe WbmF Arg296 and Trp298 Cα carbons 18 Å away from Mth375 Arg281 and Trp283 Cα atoms. WbmF active sites also contain a second positionally conserved basic side chain [34], equivalent to Mth375 Asn197 and not in the position occupied by the hydrophobic residue Phe89. Mth375 unlike other previously described WbmFs possesses the catalytic Ser129 suggesting that it could act as an oxidoreductase and/or a 3,5-epimerase [34].

To investigate potential substrate binding of Mth375, docking analysis was performed for the following molecules UDP-*N*-acetylglucosamine (UD1), UDP-glucose (UPG), UDP-glucuronic acid (UGA) and UDP-*N*-acetyl-D-glucosaminuronate (HP7) on NADH and UDP bound Mth375 using the *in silico* docking software GOLD [39]. The Asn91, Asn184 and Asn197 side chains were allowed the most rotameric freedom during docking to accommodate binding of the larger sugar bound UDP molecules, with the resulting top ranked poses depicted in Fig. 3C. The binding poses of the pyranose sugars of each potential substrate were near identical, and the large rotameric movements of Asn184 and Asn197 allowed for the best induced fit and reduced clash scoring for each molecule. UD1 scored best followed closely by UPG, ranked first and second amongst the docked poses, while HP7 and UGA ranked tenth and nineteenth, respectively. The orientation of UPG closely mimicked that seen in 1EK6, which could suggest that 4-epimerisation is possible but would require a large rotameric movement of Asn91. As previously stated, however, this would not be possible for the even larger acetylated or carboxylated substrates. The lower rankings of HP7 and UGA poses may be due to interactions of the carboxylate atop a small hydrophobic pocket created in part by residues Cys131, Phe183 and Leu289; however, hydrogen bond interactions with the sidechain hydroxyl of Ser129 and the sidechain carbonyl of Asn184 may ameliorate any nonoptimal binding. Similarly, the hydroxyl of UD1 in the same position can make hydrogen bond interactions with the same residues. Overall, each molecule docked into Mth375 produced reasonable binding of near identical poses, making a definitive annotation of activity inconclusive; however, we can eliminate UD1 epimerisation.

Crystal structures of Mth373

Mth373 expressed with a yield of 4.1 mg·L^{-1} culture and eluted as a single peak from nickel-affinity purification with purity appropriate for protein crystallisation (in excess of 95% as assessed by SDS/PAGE).

Table 2. A topology-based assessment of Mth375 structural homologues utilising CLICK [37].

Rank	Homologous structure	Z-score	Structural overlap (%)	RMSD (Å)	#identical residues	Homologue description	Gene name/ mutation[a]	EC[a]	Substrate[a]	Organism
1	3RUF-A	9.02	93.71	1.28	92	WbgU	WbgU	5.1.3.7	UDP	*Plesiomonas shigelloides*
2	2P5Y-A	8.75	92.93	1.28	90	UDP-glucose 4-epimerase	TTHA0591	5.1.3.2	–	*Thermus thermophilus*
3	2B69-A	8.31	92.72	1.39	92	UDP-glucuronate decarboxylase 1	UXS1	4.1.1.35	UDP	*Homo sapiens*
4	1SB8-A	8.24	91.92	1.42	88	WbpP	–	5.1.3.7	UD2	*Pseudomonas aeruginosa*
5	3VPS-A	7.93	93.40	1.51	79	NAD-dependent epimerase/ dehydratase	TunA	4.2.1	UD1	*Streptomyces chartreuses*
6	3KO8-A	7.92	92.59	1.52	71	UDP-galactose 4-epimerase	GalE	5.1.3.2	–	*Pyrobaculum calidifontis*
7	2Q1S-A	7.62	85.03	1.35	109	Putative nucleotide sugar epimerase/dehydratase	WbmF	–	–	*Bordetella bronchiseptica*
8	3ENK-A	7.43	87.43	1.44	80	UDP-glucose 4-epimerase	GalE	5.1.3.2	UPG	*Burkholderia pseudomallei*
9	1EK6-A	7.34	89.22	1.54	80	UDP-galactose 4-epimerase	GalE	5.1.3.2, 5.1.3.7	UPG	*Homo sapiens*
10	1KEW-A	7.24	91.02	1.53	84	dTDP-glucose 4,6-dehydratase	RmlB	4.2.1.46	TYD	*Salmonella typhimurium*
11	4LIS-A	7.21	87.13	1.49	90	UDP-galactose 4-epimerase	GalE	5.1.3.2	UPG	*Aspergillus nidulans*
12	1OC2-A	7.21	90.12	1.56	84	dTDP-glucose 4,6-dehydratase	RmlB (RfbB)	4.2.1.46	TDX	*Streptococcus suis*
13	1R6D-A	7.20	90.99	1.58	91	dTDP-glucose 4,6-dehydratase	desIV/D128N, E129Q	4.2.1.46	DAU	*Streptomyces venezuelae*
14	2PK3-A	7.18	89.64	1.59	66	GDP-6-deoxy-D-lyxo-4-hexulose reductase	RMD	1.1.1.281	GDD	*Aneurinibacillus thermoaerophilus*
15	1UDC-A	7.00	86.83	1.54	82	UDP-galactose 4-epimerase	GalE	5.1.3.2	UFM	*Escherichia coli*

[a]As annotated in the RCSB (https://www.rcsb.org/).

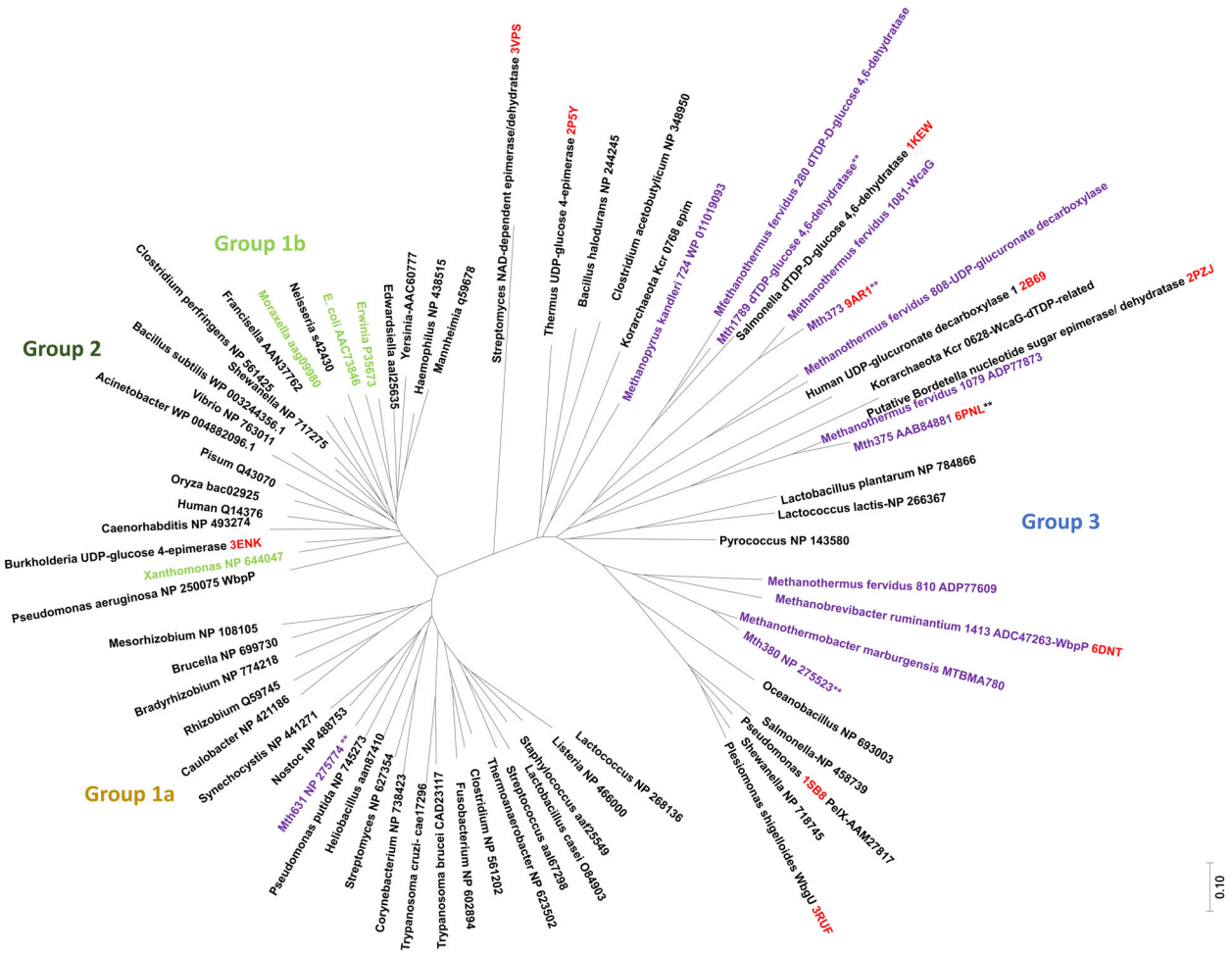

Fig. 4. A phylogenetic tree of archaeal SDR's. Neighbour-Joining [74] phylogenetic tree of methanogen 4-epimerases together with Group 1-3 proteins from the phylogenetic analysis by Ishiyama *et al.* [36]. Sequences for crystal structures of relevant 4-epimerases discussed in this text are also included for reference (highlighted in red text). Group names are coloured to match those of Ishiyama *et al.* [36] using the following colour-coding: Group 1a (mustard); Group 1b (light green); Group 2 (dark green); and Group 3 (blue). Group 1b sequences are shown in light green text and are interspersed with Group 2 sequences. Methanogen epimerase branches are shown with lavender text, and epimerases that had their structures determined or modelled in this study are indicated with asterisks (**). Seventy-two amino acid sequences were downloaded from the non-redundant NCBI or RCSB databases and imported into MEGA7 [75]. The sequences were aligned using Clustal Omega (0.1.2.4) [38] and a Neighbour-Joining phylogenetic tree [74] constructed in MEGA7 using default parameter settings [75]. The tree is drawn to scale, with branch lengths in the same units as those of the evolutionary distances used to infer the phylogenetic tree. The evolutionary distances were computed using the Poisson correction method [78] and are in the units of the number of amino acid substitutions per site. All positions containing gaps and missing data were eliminated. There was a total of 208 positions in the final dataset.

Mth373_NU crystallised in the orthorhombic space group *P 2 2 21* with unit cell parameters a = 54.5 Å, b = 81.4 Å, c = 152.4 Å, α = β = γ = 90.0° and solvent content 46% (Matthews coefficient of 2.29 Å^3·DaÅ^3·Da^{-1}). Mth373_NX crystallised in space group *H 3 2* with unit cell parameters a = 139.3 Å, b = 139.3 Å, c = 226.9 Å, α = β = 90° and γ = 120° and a solvent content of 59% (Matthews coefficient of 3.03 Å^3·Da^{-1}; see Table 1 for diffraction data and refinement, Mth373_NU and Mth373_NX statistics). Both Mth373 complexes crystallised as a dimer within the asymmetric unit (Fig. 5A,B), with an average total buried surface of 8631.7 Å^2 and a calculated dissociation complex ΔG°_{diss} of 20.7 kcal·mol^{-1} [35]. Electron density maps for both Mth373 structures displayed unbroken electron density throughout the main chain of each 311-residue monomer apart from Glu60 and a few instances of side chain disorder, which for

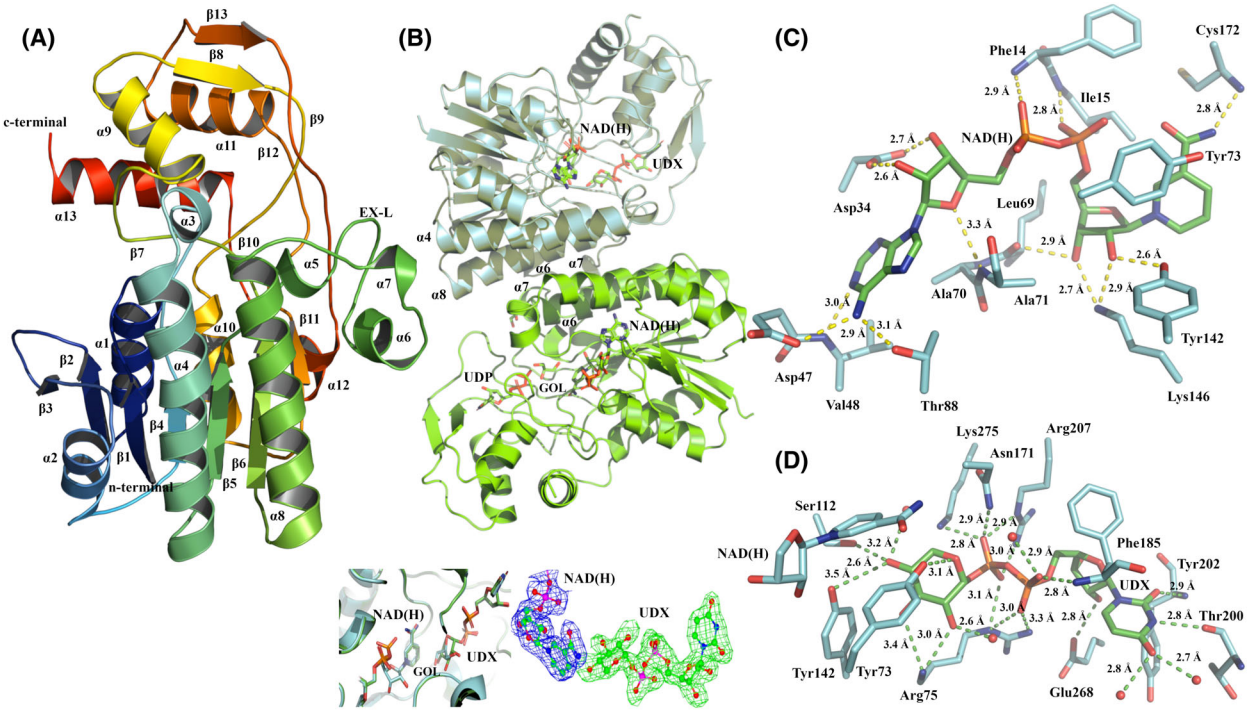

Fig. 5. Structures of *M. thermautotrophicus* ΔH Mth373. (A) A ribbon representation of methanogen Mth373_NX (EC 4.1.1.35/4.2.1.46) with secondary structural elements labelled. The structure is colour-ramped from the N terminus (blue) to C terminus (red). (B) Dimeric ribbon representation of Mth373_NX. Important secondary structure elements α4, α8, α6 and α7 are labelled. Inset bottom left: the Mth373_NX monomers are superimposed illustrating the binding modes of GOL and UDX in the active site of the enzyme alongside an omit electron density map (Fo-Fc) of bound UDX (in green). (C) The coenzyme (NAD(H)) binding domain of Mth373_NX (carbon atoms in cyan). (D) The active site of Mth373_NX with bound UDX (carbon atoms green). Relevant residues and water molecules within 4 Å of UDX and NAD(H) are depicted. Polar contacts with distances are indicated as dashed lines. All figures were prepared using PyMOL version 2.5.8.

Mth373_NX was predominantly at the C terminus. Both complexes have interpretable electron density for a molecule of NADH in the N-terminal coenzyme-binding domain (Fig. 5C) of each monomer and a molecule of UDP in each of the active site domains of Mth373_NU, but in only one of the active site domains of Mth373_NX. Co-crystallisation with UGA failed to show binding to the structure; however, the active site domain of Mth373_NX contained electron density indicative of a bound uridine-5′-diphosphate-xylopyranose (UDP-xylose, UDX; Fig. 5D). For both Mth373 complexes, the UDP and NADH molecules superimpose in an identical manner, so results and discussion will centre exclusively on Mth373_NX. The electron density map is depicted in Fig. 5 for the bound UDX molecule.

Mth373, like the aforementioned Mth375 and other archaeal, bacterial and eukaryotic 4-epimerases [24,26,33] of the SDR superfamily, shares a common architecture with an N-terminal nucleotide-binding domain predominantly formed by a modified Rossmann-fold motif (residues 1–168), binding NADH, and a C-terminal active site domain that binds the UDP-sugar substrate (residues 169–311; Fig. 5A). The N-terminal domain is formed by seven parallel β-strands (residues 4–10 β_1, 29–34 β_2, 42–46 β_3, 64–69 β_4, 105–110 β_5, 163–168 β_6 and by C-terminal domain residues 230–234 β_{11}) and ten α-helices (residues 13–26 α_1, 50–61 α_2, 75–80 α_3, 82–104 α_4, 112–117 α_5, 126–130 α_6, 133–137 α_7, 140–161 α_8 and C-terminal domain residues 213–225 α_{10}, and 280–285 α_{12}). The parallel β-strands are sandwiched on one side by α-helices α_2, α_4, α_5, α_6, α_7 and α_8 on the other by α-helices α_1, α_{10} and α_{12}. The extended coenzyme-binding motif ***G***-*X*-*X*-***G***-*X*-*X*-***G*** is located on the short loop between β_1 and α_1 (coenzyme loop 1; residues 10–16) with sequence ***G***-*G*-*A*-***G***-*F*-*I*-***G***. Coenzyme loop 2 in Mth373 is shorter than in Mth375, making fewer contacts with the coenzyme (residues 34–36) and is located between β2 and β3. Coenzyme loop 3 is formed between β_3 and on α_2 (with residues 46–49) and coenzyme loop 4 falls between β_4 and on α_3 (residues 69–74). An extended loop (residues 112–124) that incorporates a short alpha helix (α_5) also

straddles both the substrate and coenzyme-binding domains and is formed between β_5 and α_6. The C-terminal domain of Mth373 is comprised of six very short β-strands (formed by residues 171–173 β_7, 199–203 β_8, 205–207 β_9, 210–211 β_{10}, 242–243 β_{12} and 261–265 β_{13}) and three large α-helices (formed by residues 184–195 α_9, 244–256 α_{11} and 293–309 α_{13}). The catalytic motif of the enzyme is located on α_8, with sequence ***Y-A-I-T-K*** (residues 142–146, α_8) [24,31]. Interactions with the UDP-bound sugar are depicted in Fig. 5D and are maintained in part by secondary structure elements α_5, α_8, α_9, α_{11} and β_8, and the active site loop between β_4 and α_3. Overall, the dimeric structure of Mth373 is formed via several hydrogen bond networks including the interactions between residues of the adjacent helices of α_6 and α_7 and via the anti-parallel stacking of helices α_8 and α_4 (Fig. 5B). This latter interaction also forms a water-excluding hydrophobic patch created by residues Ile144, Ala148, Leu151 and Met152 on α_8 and Val90, Ile91 and Trp86 on α_4. Additional salt bridges between monomers are maintained primarily by the side chain of Glu79 (OE1, α_3) and the side chain of Lys94 (NZ; 2.80 Å, α_4) and Arg98 (NH2; 3.26 Å, α_4), and the side chains of Asp141 (OD1, α_8) and Lys94 (NZ; 2.81 Å, α_4).

The Mth373 to NAD(H) coenzyme molecular interactions are depicted in Fig. 5C. The conserved coenzyme-binding motif (sequence ***G-G-A-G-F-I-G***) main chain amines Gly13 (N), Phe14 (N) and Lys183 (N) make hydrogen bond contacts with the NADH pyrophosphate bridge and ribose sugar. The shortened NAD(H)-binding loop interacts with the NADH adenine via a π-stacking interaction (Leu35), while the NADH ribose hydroxyls form hydrogen bond contacts with Asp34 (OD1 and OD2). The ribose ring oxygen of the adenosine moiety forms an additional hydrogen bond interaction with the main chain of Ala71 (N) while the adenine base forms hydrogen bond contacts with the main chain of Val48 (N), the side chain of Asp47 (OD1) and the side chain of Thr88 (OG1). The ribosylnicotinamide forms hydrogen bond contacts via Leu69 (OÅ), Tyr142 (OH), Lys146 (NZ) and Cys172 (N). A π-stacking interaction is also observed via the mostly conserved side chain of Tyr73, which is immediately adjacent to the catalytic Tyr142 and the nicotinamide ring of NADH.

A single molecule of UDP was bound to each active site of the Mth373_NU dimer. For Mth373_NX, one monomer contained UDP and additional density consistent with a single molecule of glycerol in the sugar-binding domain, while the second monomer contained electron density refined as uridine-5′-diphosphate-xylopyranose (UDP-xylose, UDX; Fig. 5). Mth373 apo preparations and subsequent crystallisation always resulted in complexes with clearly bound coenzyme and little to no clear electron density corresponding to the presence of bound substrate (results not shown). It is unknown if the observed UDP-xylose (UDX) molecule bound in Mth373_NX is a result of enzymatic activity or decarboxylation of bound UDP-glucuronic acid (UGA) during synchrotron data collection, or a combination of the two in a mechanism where the Mth373 active site has strained the UDP-glucuronic acid carboxylate so that it is more prone to radiation effects [40]. Similarly, we cannot explain why one active site domain of Mth373_NX possesses a single UDP molecule and glycerol (see inset panel of Fig. 5B). Glycerol is not present in the nickel-affinity purification steps; it is not in the storage buffer, mother liquor or cryoprotectant and was not seen in other crystallisation experiments with the enzyme.

The diphosphate moiety of UDX forms several hydrogen bond interactions including Asn171 (ND2), Lys275 (NZ), Arg207 (NE and NH2), Arg75 (NH2and NE) and Phe185 (N) and water molecule O27. The uridine ribose hydroxyls form hydrogen bond contact with the side chain carboxylate of Glu268 (OG), while the carbonyl groups present on the uracil moiety make hydrogen bond interactions with Tyr202 (N) and waters O587 and O649, while the 2′-amide forms a hydrogen bond with Thr200 (O). The hydroxyls of the UDX UDP-xylose make hydrogen bond contacts with Arg75 (N), the side chain hydroxyls of Ser112 (OG), Tyr142 (OH) and water molecules O528 and O555, while the oxygen of the pyran ring forms a hydrogen bond contact with the side chain hydroxyl of Tyr73 (OH).

Probing the sugar-binding domain of Mth373

Mth373 clades with the *Salmonella enterica* structure PDB: 1KEW annotated as a dTGD (EC 4.2.1.46; [41]), the human UDP-glucuronate decarboxylase PDB: 2B69 (EC4.1.1.35) and the WcaG family of epimerases. The active site of Mth373 depicts the largely conserved catalytic triad [42] of Lys146, Tyr142 and Ser112 with ConSurf analysis of residues immediately around the xylopyranose sugar of UDX also showing a remarkable level of conservation (see Fig. 6A). The only real exception being a residue immediately adjacent to the catalytic triad, Tyr73 (typically conserved as phenylalanine) and Gly184 (typically conserved as serine). These residues are present on flexible loops known to contribute to substrate binding [43] including the immediate loop region preceding α3 (residues 73–76) and an elongated loop

between β7 and α9 (residues 174–183), which may indicate a paired substitution of function for the two residues to stabilise substrate binding with the hydroxyl group now provided by Tyr73 instead of serine as found in homologues. The presence of this second tyrosine immediately adjacent to the catalytic domain and the nicotinamide of the NADH is a unique feature of the Mth NS-SDRs, as is the positioning of its side-chain hydroxyl within 3.0 Å and 3.3 Å of the C4 and C5 positions of the UDX xylopyranose moiety. However, other SDRs involved in UGA decarboxylation reactions, notably UDP-D-apiose/UDP-D-xylose synthase from *Arabidopsis thaliana* (UAXS; [44], PDB: 6H0N), human UDP-α-D-xylose synthase (UXS; [43]; PDB: 4GLL and PDB: 2B69) and ArnA, a Gram-negative bacteria UGA decarboxylase involved in lipopolysaccharide synthesis ([45]; PDB: 2BLL) do possess several key similarities (summarised in Table 3) outside of the catalytic residues such as a second active site tyrosine. The equivalent tyrosines of PDB: 4GLL, PDB: 2BLL and PDB: 6H0N are found within a helix equivalent to the α3 helix of Mth373, while Tyr73 of Mth373 is present on the preceding loop. This is the same location as Cys100 of PDB: 6H0N, a key residue involved in substrate proton transfer and glucuronic acid ring opening during catalysis [44]. This process occurs prior to decarboxylation which is followed by either sugar ring contraction to form a UDP-apiose or without contraction to form UDP-xylose. Other identically positioned residues between these homologues include asparagine and glutamine residues, with the latter playing an important role in the relay of protons during catalysis driving the decarboxylation reaction [44,45]. PDB: 4GLL, PDB: 2BLL and PDB: 6H0N have two identically positioned arginines with one of these replaced by Lys275 (in contact with the UDX diphosphate moiety) in Mth373. Arg75 present on Mth373 α3 replaces the interactions observed in the second conserved Arg site, making a larger number of hydrogen bond interactions with the substrate than that seen in PDB: 4GLL, PDB: 2BLL and PDB: 6H0N. Arg75 also makes a salt bridge with Glu268, configuring/stabilising the Mth373 active site. Overall, the most likely functional assignment for Mth373 is as a UDP-xylose synthase (EC4.1.1.35) based on sequence analyses and the presence of UDP-xylose in the Mth373_NX structure, with Tyr73 facilitating proton transfer and/or stabilising the transition state of the substrate, combined with Glu114, to drive UDP-xylose formation, and that the oxidative decarboxylation of the UGA does not likely involve cleavage of the glucuronic acid ring as is seen for PDB: 6H0N.

Probing the sugar-binding domain of Mth1789, Mth631 and Mth380

Pseudomurein cell wall production requires a number of enzyme activities to convert sugar precursors to the glycan component of pseudomurein [15,16,18] with *M. thermautotrophicus* ΔH possessing several enzymes that could play these roles. These include Mth373 and Mth380 which are in two juxtaposed gene clusters (Mth370-Mth378 and Mth379-Mth381) annotated as encoding proteins involved in extracellular carbohydrate metabolism. The presence of Mth373 and Mth380 in these two *M. thermautotrophicus* gene clusters, along with Mth1789 and Mth631, strongly suggests that they play differing or overlapping roles in extracellular carbohydrate metabolism. Substrate specificity within the NS-SDRs is primarily the result of the dynamic protein flexibility seen in residues coordinating their sugar substrates and catalytic intermediates, with as little as one amino acid change potentially altering the substrate specificity and classification of the enzyme. Structural alignment of the Mth1789, Mth631 and Mth380 models, combined with the Mth375 and Mth373 crystal structures demonstrates this, with the Tyr and Lys catalytic residues (Fig. 6B italicised blue region) being the only strictly conserved active site residues across all these *M. thermautotrophicus* enzymes, apart from an Asn (orange region). A catalytic Ser is observed in Mth373 and Mth375 and is a Thr in Mth1789, Mth631 and Mth380 (mustard yellow region).

A number of studies [36,46–48] have identified common catalytic residues amongst UDP-glucose 4-epimerases (the S/T, Y, K triad; residues Ser129, Tyr155 and Lys159 in Mth375) and established the idea of 'gatekeeper' residues that mediate the propensity for acetylated or nonacetylated UDP-sugar substrates by significantly changing the volume of the sugar-binding domain. This includes studies by Guo *et al.* [48] which showed that mutagenesis of the *E. coli* UDP-glucose 4-epimerase Ser306 to a tyrosine reduced activity with nonacetylated substrates by fivefold and completely removed activity with acetylated substrates. Furthermore, 4-epimerases can be delineated into groups with differential preferences for their substrates [33,36,49]. Group 1 enzymes prefer nonacetylated substrates, Group 2 enzymes do not show a strong preference for either acetylated or nonacetylated substrates, while Group 3 shows a preference for acetylated substrates [36]. A phylogenetic tree of hexose 4-epimerase sequences was constructed from Groups 1–3 [36] together with methanogen sequences and those for some recently described crystal structures (Fig. 4) in order to inform the substrate specificity of the Mth

(A)

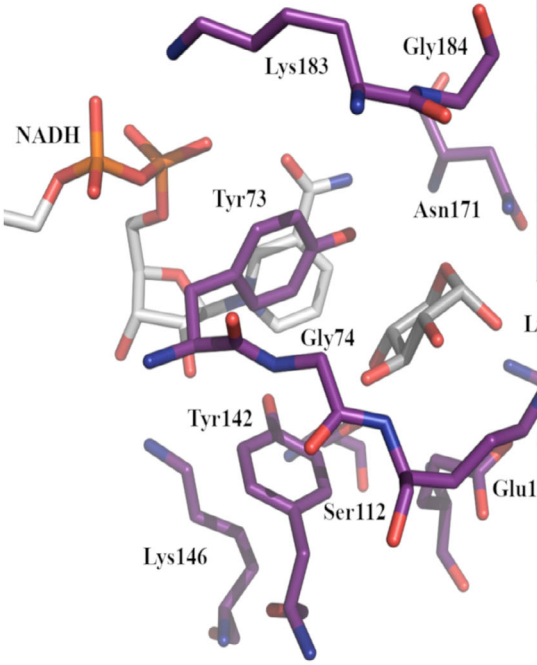

Amino Acid	% occurrence of amino acids in the equivalent position		
Y73	Y 73.83	F 25.5	S 0.67
G74	G 100		
R75	R 100		
S112	S 99.3	T 0.7	
E114	E 100		
Y142	Y 100		
K146	K 100		
N171	N 94	G 6	
K183	K 88.67	R 10.67	A 0.67
G184	G 74.7	S 25.3	
K275	K 100		

(B)

```
                                                                                                                  62
MTH380  ------------MRDMDVAVTGGLGFIGSHLTDELLERGN-RVTVIDDL-S-TGSP-DNL-RDPHHEDLEII-E
MTH1789 M---------------EKILVTGGAGFIGSNFIRYMLQEHPYHIINLDAL-TYCGNL-ENLRGVEDEPRYTFV-R
MTH631  -----------------MILIVGGAGYIGSHVNKFLSERGY-ETLILDNL-TR-GHR-DFV--KWG-----EFIE
6PNL    -----MIMDEFRAYDGKCVLVTGGAGCVGSNLTGNLAKAGA-NVIILDNL-S-SSYE-WNI-PE--YENIEFV-K
9AR1    --------------T-QRILVTGGAGFIGTNLVNELRNRGH-EVLAVDLMH-----TE------RE----DYM-R
                          :::**:* :*:     :   :       * :
                                                                                                                 135
MTH380  GSIND--LDLEKVFQ--GKDYVFHQAALASVPESVRDPLRCHRVNATGTLRVLMASSRAGVRKVVNASTSAV-YG
MTH1789 GSITDRKLVD-GIIK--DVDAVINFAAESHVDRSIEDPEIFIRTNILGTQTLLEASRKHGVERFIQISTDEV-YG
MTH631  GNLGDRRLLD-RTFETHDVDAVMHFAAFTDVGESVLKPGRYYHNNVVNTINLLDSMVDHGVRDFIFSSTCAV-YG
6PNL    GDILDDEVLK-RVFK-ERPDYVFHLAAHFANQNSVDNPEKDLLVNGLGILKVLEYAQLVGVERFVYSSSGCGVYG
9AR1    ADVREYRQVE-RIFEEDKFDYVYHLAAEYGRWNGEDYYENLWKTNVIGTKHMLRMQEKLGF-RMIFFSSAEV-YG
        :   :         :     * * : **       :   :       *  ::   *      *:       *   : **
                                                                                                                 195
MTH380  NNP-EIPLREDAR-------P-MPLSPYAVSKVTGEYYCQVFED-QGLETVSLRYFNVYGP------RQRPDSQY
MTH1789 S-AEKGYFTEETP-------L-APNSPYSASKASADLMVRAYHRTYGLPVNITRCSNNYGP------YQFP----
MTH631  NPM-EIPISEEHP-------L-NPISPYGRSKLMVEEILGDYRDAYGLNYVSLRYFNAAGADPEGEVGELHNP-E
6PNL    LDS-KIPFEEHDI-------SISLHTPYQVTKLLGELYTNYFHNLYEMPIVNARFFNVFGP------GEVPGK-Y
9AR1    DYS-G-LMSEDVMVKNPISDT-YQMNDYAITKWAGELMCMNSAEMFGTETVRVRPVNCYGP------HEKYSP-Y
              *                :*   *    :         :   :  *  *  *:
                                                                                                                 259
MTH380  AAVIPRFIDALLS-GRSPEIYGDG-------EQSRDFIYVGDVVRANIFLAESR-GS--GVYNVA-GG-SSVTVN
MTH1789 EKLIPLMITNALE-NKPLPVYGDG-------MNVRDWIHVLDHCRAVDLVLHRG-RVG-EVYNIG-GN-SERRNI
MTH631  THLIPIVLDVALGLRDAVRI-FGTDYPTPDGTCVRDYIHVMDLADAHWRALRYLEGGESGVFNLG-NG-NGFSVM
6PNL    RNVIPNFFYWAMN-QQPLPITGDG-------SETRDWTFVEDIVRGLMAMGVRREAIG-EAINLG-SG-TEHQVI
9AR1    KGFIPIFIYHALH-RKPYTV-Y-K-------GHKRIIDYVEDSVRTFANIVDNF-IPG-EVYNVGGRTEWEHDIK
           **     :                       *    * *  :               : * :
                                                                                                                 325
MTH380  RLFDIISGILESDAE--PEYL-DERPGD-V-RHSLADTSRL-A--AAGFRPEVG-L-EEGLMRTVEWFLERLK-
MTH1789 EIVELIVRELGKD-ESLIRFV-EDRPGH-D-RRYAIDASKIRN--ELGWKPL-Y-SFEEGIRETIRWYIDNRD-W
MTH631  EVIETCREVTGASI--NAVED-DRRP--GDPPELVGSAGRARRVL--GWRPE-FTELEDIIETAWNWHSRIR--G
6PNL    EMAGIINELTENPAG--VVYR-PRRDWDAK-TRLLSSIDKARR--LLDYEPQ-V-SFREGLERTHRWFTENWE-L
9AR1    EYSDMVLEAVGID-DSIVTYRE-SEPFT-T-KVKTMDFSKAIR--DLKHDPQ-V-PPEEGIRRTVEWMKWYYRI-
        :                      ::                          *      :::   :  *
              332
MTH380  --------*
MTH1789 WEN--IK-*
MTH631  G--IS---*
6PNL    IRKS-AEF*
9AR1    --------*
```

Fig. 6. The substrate binding domain of Mth373. (A) ConSurf analysis of Mth373 [73]. The table details the residues in % conservation terms for Mth373 amino acid position within the sugar-binding domain of the enzyme. The matching conserved residue is shown in red with decreasing conservation values from left to right in columns 2–4. (B) The *M. thermautotrophicus* ΔH enzyme structures Mth380 (accession number O26480), Mth1789 (accession number O27817), Mth631 (accession number O26728), Mth375 (PDB: 6PNL; accession number O26475) and Mth373 (PDB: 9AR1; accession number O26473) were superimposed using SALIGN [72]. The resultant sequence alignment was calculated by Clustal Omega (0.1.2.4) multiple sequence alignment online server [38]. Identical residues are indicated with a '*'. The catalytic residues are in blue indicating the characteristic signature sequence *Y-X-X-X-K* of short-chain dehydrogenases/reductases, while the coenzyme signature sequence *G-G-X-G-X-X-G* is in green. Each substrate binding domain within 5 Å of a bound UDP-sugar is also highlighted and shaded to match groups previously delineated and colour coded (red, mustard yellow, blue, orange, purple, grey, dark green) [36,52]. Numbering is based on the PDB: 6PNL crystal structure. Structure figures were prepared using PyMOL version 2.5.8.

Table 3. Comparison of UDP-xylose synthases, catalytic and selective active site residues along with the proposed catalytic mechanisms.

Mth373	2B69/4GLL	2BLL	6H0N
M. thermautotrophicus ΔH	*Homo sapiens*	*Escherichia coli*	*Arabidopsis thaliana*
UDP-xylose synthase	UXS	ArnA	UAXS
EC4.1.1.35	EC4.1.1.35	EC4.1.1.35	
Reaction	Reaction	Reaction	Reaction
UGA oxidative decarboxylation	UGA oxidative decarboxylation	C4′ hydride abstraction (oxidation) and subsequent decarboxylation	NAD(H) linked oxidation and reduction Aldol cleavage/Sugar ring opening UGA decarboxylation aldol-linked substrate contraction and furanosyl production/aldol-linked pyranosyl production
Catalytic triad	Catalytic triad	Catalytic triad	Catalytic triad
Lys146	Lys151/235	Lys467	Lys189
Tyr142	Tyr147/231	Tyr463	Tyr185
Ser112	vThr118/202	Thr432	Thr139
Aligned signature residues	Aligned signature residues	Aligned signature residues	Aligned signature residues
–	Tyr84/168	Tyr398	Tyr105
Glu114	Glu120/204	Glu434	Glu141
Arg75[a]	Arg144/228	Arg460	Arg182
Lys275	Arg277/361	Arg619	Arg341
Asn171	Asn176	Asn492	Asn214
Tyr73	Ala79/Ala163	Ala393	Cys100
Ala113	Ser119/Ser203	Ser433	Cys140

[a]Not in identical sequence position.

enzymes. Our updated analysis shows the epimerase sequences separating into three main clades similar to those described by Ishiyama [36]. Mth631 is embedded in Group 1a sequences which supports its designation as a GalE epimerase. Mth1789 clades closely with PDB: 1KEW in Group 3 indicating it to be a dTDP-D-glucose 4,6-dehydratase. Mth380, also in Group 3, clades closely with the previously characterised *Methanobrevibacter ruminantium* 1413 (PDB: 6DNT) [26] which is designated a UDP-*N*-acetylglucosamine 4-epimerase (WbpP; EC5.1.3.7).

Summarised in Table 4 are the sugar-binding and active site motifs of the *M. thermautotrophicus* enzymes that were modelled using Molsoft [50,51], their functional annotations and model template details, in comparison to the crystal structures of Mth375 and Mth373. Amongst the modelled proteins, only Mth1789 had an identical amino acid fingerprint to other published dTGDs (EC4.2.1.46) [52]. It was modelled using the *Streptomyces venezuelae* dTGD structure (PDB: 1R66; [53]) sharing a 53% structural identity and a 90% active site homology. Mth380 was modelled utilising the crystal structure of *Methanobrevibacter ruminantium* M1 UDP-*N*-acetylglucosamine 4-epimerase (Mru1413; WbpP; EC5.1.3.7; PDB: 6DNT; [26]) with which Mth380 shares the highest sequence identity (55%) of published structures. The signature key residues of Mth380 Ala81, Ser82, Val83, Tyr145, Asn173, Ala187 and Ser276 share high sequence identity with another UDP-GlcNAc 4-epimerase, (WbpP;

Table 4. Sugar-binding motifs of the NS-SDRs of *M. thermautotrophicus*. Groups have been previously delineated [36,52] and colour coded to match.

Substrate binding motifs							
Enzyme	Structure/coenzyme/ substrate		Catalytic residues (YX_3K)			Gate keeper residues	Details
Mth375 [34] Group 3	PDB: 6PMH, 6PNL/ NAD/UDP	$_{88}$HFANO$_{92}$	$_{128}$SGC$_{131}$	$_{155}$YQVTK$_{159}$	$_{182}$FFNV$_{185}$	$_{190}$EVPGKYRNV$_{198}$	$_{220}$ETRDW$_{224}$	$_{284}$DAKTRL$_{289}$	Name; WbmF putative nucleotide sugar epimerase/ dehydratase EC–; Substrate: –
Mth373 Group 3	PDB: 8W3U, 9AR1/ NAD/UDP, UDX	$_{72}$EYGRW$_{76}$	$_{111}$SAE$_{114}$	$_{142}$YAITK$_{146}$	$_{169}$PVNC$_{172}$	$_{177}$EKYSPYKGF$_{185}$	$_{205}$HKRII$_{209}$	$_{271}$TTKVK$_{275}$	Name; UDP-xylose synthase EC 4.1.1.35; Substrate: UDP-glucuronic acid
Mth1789 [52] Group 3	Molecular model (PDB: 1R66)/NAD/TYD, DAU	$_{82}$ESHVD$_{86}$	$_{123}$TDE$_{125}$	$_{147}$YSASK$_{151}$	$_{174}$CSNN$_{177}$	$_{182}$QFPEKL$_{187}$	$_{209}$NVRDW$_{213}$	$_{273}$HDRRY$_{277}$	Name; dTDP–D-glucose 4,6-dehydratase EC 4.2.1.46; Substrate: –
Mth380 [36,76] Group 3	Molecular model (PDB: 6DNT)/NAD/EPZ	$_{81}$ASVP$_{84}$	$_{120}$TSA$_{123}$	$_{143}$SPYAVSK$_{149}$	$_{171}$YFNV$_{174}$	$_{179}$QRPDSQYAA$_{187}$	$_{210}$QSRDF$_{214}$	$_{272}$DVRHS$_{276}$	Name; WbpP EC 5.1.3.7; Substrate: UDP-*N*-acetylgalactosamine
Mth631 Group 1a	Molecular model (PDB: 2C20)/NAD/–	$_{77}$FTDVG$_{81}$	$_{117}$TCA$_{120}$	$_{142}$YGRSK$_{146}$	$_{169}$YFNA$_{172}$	$_{183}$ELHNPETHL$_{191}$	$_{220}$CVRDY$_{224}$	$_{285}$GDPPEL$_{290}$	Name; GalE EC 5.1.3.2; Substrate: UDP-glucose

EC5.1.3.7; PDB: 1SB8; [36]) and are identical to PDB: 6DNT [26]. The phylogenetic analysis (Fig. 4) showed that Mth373 clades with a number of UDP-glucuronate decarboxylases (EC4.1.1.35), dTGD (EC 4.2.1.46; O26473_METTH) and other 3,5-epimerising oxidoreductases identified as WcaGs that nominally catalyse the formation of GDP-L-fucose from GDP-4-dehydro-α-D-rhamnose in *E. coli* (GDP-4-keto-6-deoxymannose-3,5-epimerase-4-reductase; EC1.1.1.271) [54–56]. Mth631 is the classical *M. thermautotrophicus* GalE as it does not clade with any enzymes involved in acetylated UDP-hexose metabolism, and structural and sequence analysis showed that this enzyme best aligns almost exclusively with other GalEs; for example, from *B. anthracis*, (PDB: 2C20) with a 50% total structural identity and an 88% identity amongst the residues that form contacts with the glucose sugar of UPG.

Conclusions

We present the first crystal structures of Mth375 a WbmF, and Mth373 (EC4.1.1.35) alongside the structural analyses of Mth380 a WbpP (EC5.1.3.7), Mth1789 a dTGD (EC4.2.1.46) and Mth631 a GalE (EC5.1.3.2) that enable the structural and functional annotation of the *M. thermautotrophicus* ΔH NS-SDRs. It should be noted that archaea such as *Methanopyrus kandleri* (strain AV19) only possess a single identifiable 4-epimerase (MK724), which clades with Group 3 enzymes involved in acetylated UDP-hexose metabolism. It is therefore likely that Group 3 enzymes are involved in *N*-acetyltalosaminuronic acid production, the unique archaeal sugar moiety of pseudomurein [15–19]. This is unlikely to include Mth373 decarboxylation reactions. The results presented here suggest that these enzymes have multiple activities to facilitate methanobacterial pseudomurein and capsular polysaccharide production. Future activity studies on these enzymes would confirm the exact/specific role each plays.

Materials and methods

Materials

Analytical reagents and chemicals were purchased from Sigma-Aldrich (St. Louis, MO, USA), Fluka (Ronkonkoma, NY, USA) and Merck (St. Louis, MO, USA). Crystallisation buffers and kits were purchased from Hampton Research (Aliso Viejo, CA, USA) and Molecular Dimensions (Rotherham, UK). *N*-acetyl-D-glucose, *N*-acetyl-D-galactose, *N*-acetyl-D-glucosamine and *N*-acetyl-D-galactosamine were obtained from Sigma-Aldrich.

Cloning, expression and purification of Mth375 and Mth373

Methanothermobacter thermautotrophicus ΔH (DSM 1053) was obtained from the Leibniz Institute DSMZ (Braunschweig-Süd, Germany) and grown in BY^+ media at 65 °C according to Wedlock *et al.* [57]. DNA was isolated using InstaGene Matrix according to the manufacturer's instructions (Bio-Rad, Hercules, CA, USA). The *Mth375* gene was amplified using forward primer 5′-CACCTTG ATTATGGATGAATTCAGGGCTA and reverse primer 5′-TTAGAACTCTGCGCTCTTCCTTATG in pET100D (Invitrogen, Carlsbad, CA, USA). The forward primer contained a 5′-CACC sequence for topoisomerase-mediated cloning. The positive clone plasmid DNA was sequenced at Massey University Genome Service to confirm the cloned *Mth375* gene sequence was correct. Mth375 was expressed as a recombinant hexahistidine-tagged protein in *E. coli* BL21-Rosetta 2 (Novagen, Madison, WI, USA) at 28 °C and purified using protocols previously described [26], with the following changes made. The lysis buffer was 50 mM Tris pH 7.5 containing 2 mM dithiothreitol (DTT), 300 mM NaCl, 10 mM imidazole, 1% (v/v) Triton X-100, 10 mM $MgCl_2$ and 10 μM phenylmethylsulfonyl fluoride (PMSF). The nickel-affinity equilibration buffer was 50 mM Tris pH 7.5 containing 0.3 M NaCl, 20 mM imidazole and 10% (v/v) glycerol. After purification, the buffer was exchanged by dialysis to 20 mM MOPS pH 7.0 containing 25 mM KCl, 7 mM β-mercaptoethanol and 5% (v/v) glycerol. The sample was concentrated using a 10 K Vivaspin 20 and 1 mM DTT was added.

The gene encoding Mth373 from *M. thermautotrophicus* ΔH was cloned the same as that for MTBMA1234 [26], and the protein expressed and purified as previously [26], except for the following changes. The primers used were as follows: forward 5′-CACCATGTTACCAGGAA AACCCTTATTC and reverse 5′-TCAGTCCTCTATCCT GTAGTACC. Recombinant hexahistidine-tagged Mth373 was expressed from *E. coli* LOBSTR BL21* (Kerafast, Newark, CA, USA) grown initially at 37 °C with the temperature lowered after induction to 22 °C for 16 h. After nickel-affinity purification, the buffer was exchanged by dialysis to 20 mM MOPS pH 7.0 containing 2 mM tris(2-carboxyethyl)phosphine (TCEP) and 500 mM KCl.

Crystallisation and structure determination of Mth375

Mth375 (designated Mth375_AU; 10 mg/mL in 20 mM MOPS pH 7.0, 5% (v/v) glycerol, 25 mM KCl, 7 mM β-mercaptoethanol and 1 mM DTT) was initially crystallised using the sitting drop method at 21 °C in a number of conditions using the Molecular Dimensions JCSG-plus screen and Structure Screens 1 + 2 [58]. Crystallisation was optimised via the addition of 1.0 mM uridine 5′-diphosphate (UDP) to Mth375 and for the most promising condition using the Silver Bullets Bio screen from Hampton Research. Crystals were harvested from wells with mother liquor containing 1.0 M ammonium phosphate monobasic, 0.1 M sodium citrate pH 5.6 and Silver Bullets Bio condition H9. A second solution of Mth375 (designated Mth375_NU) was prepared with 1.0 mM UDP for co-crystallisation. Crystals were obtained at 21 °C utilising the ShotGun screen from Molecular Dimensions [59] and optimised using the additive screen from Hampton Research with a resulting final mother liquor of 0.1 M NaCl, 1.6 M $(NH_4)_2SO_4$, 0.1 M sodium HEPES pH 7.5 and 3% (w/v) 1,8-diaminooctane. These crystals were then soaked in 10 mM *N*-acetyl-D-GlcN for several minutes prior to freezing in liquid nitrogen to help identify the sugar substrate binding domain. Mth375 crystals were harvested within 1-4 weeks of incubation at 21 °C. X-ray diffraction data was collected at 100 K from flash-cooled crystals in cryoprotectant containing perfluoropolyether oil for Mth375_AU or mother liquor with added 25% (v/v) ethylene glycol for Mth375_NU at the Australian Synchrotron MX beamlines [60,61] using *Blu-Ice* [62] and processed with *XDS* [63] and *Aimless* [64]. The exposure time, oscillation range, crystal-detector distance and beam attenuation were adjusted to optimise the collection of data to a resolution of 2.30 and 2.01 Å, respectively. Further data collection and processing statistics are shown in Table 1. Initial phases for Mth375_AU were determined by the molecular replacement program *Phaser* [65], within the *CCP*4 program suite [66], using the crystal structure of a sugar epimerase from the Gram-negative bacterium *Bordetella bronchiseptica* (PDB: 2PZJ) [34] as the search model. Difference-Fourier maps ($2F_o$-F_c and F_o-F_c) were visualised in *Coot* [67] and enabled the inclusion of additional amino acid side chains, associated molecules from the mother liquor and water molecules. Structural idealisation and restrained refinement were carried out using *REFMAC*5 [68]. Initial phases for Mth375_NU were determined by the molecular replacement program *MolRep* [69] using the refined crystal structure of Mth375_AU. Mth375_NU structural idealisation and restrained refinement were carried out in an identical manner to Mth375_AU. X-ray diffraction and final refinement statistics are provided in Table 1. Structural coordinates and structure factors have been deposited in the RCSB Protein Data Bank (PDB) under accession codes PDB: 6PMH (Mth375_AU) and PDB: 6PNL (Mth375_NU).

Crystallisation and structure determination of Mth373

Mth373 coenzyme bound forms (designated Mth373_NU and Mth373_NX; 4.1 mg/mL in 20 mM MOPS pH 7.0, 2 mM TCEP, 500 mM KCl and 2.0 mM NADH) were crystallised with the sitting drop method at 21 °C using the

PEGRx screen from Hampton Research. Mth373_NU contained an additional 1.0 mM UDP and Mth373_NX contained 1.0 mM uridine 5′-diphosphoglucuronic acid (UGA). Crystals were harvested from wells with mother liquor conditions 0.2 M $MgCl_2$, 0.1 M sodium citrate tribasic dihydrate pH 5.0, 10% (w/v) polyethylene glycol (PEG) 20,000 (Mth373_NU) and 0.1 M sodium citrate tribasic dihydrate pH 5.5, 18% (w/v) PEG 3350 (Mth373_NX). Crystals of either complex were harvested within 1-4 weeks of incubation at 21 °C. X-ray diffraction data were collected at 100 K from flash-cooled crystals in mother liquor containing 25% (v/v) ethylene glycol at the Australian Synchrotron MX beamlines using *Blu-Ice* [62] and processed with *XDS* [63] and *Aimless* [64]. The exposure time, oscillation range, crystal-detector distance and beam attenuation were adjusted to optimise the collection of data to a resolution of 2.00 and 1.96 Å, for Mth373_NU and Mth373_NX, respectively. Further diffraction data collection and processing statistics are shown in Table 1. Initial phases for Mth373_NU were determined by the molecular replacement pipeline *BALBES* [70] using the dTGD crystal structure from *Salmonella enterica* (PDB: 1KEW) [71], with initial automated model building and refinement using the online ARP/wARP 7.6 server [41]. Difference-Fourier maps ($2F_o$-F_c and F_o-F_c) were visualised in *Coot* [67] and enabled the addition of further amino acid side chains, associated molecules from the mother liquor and water molecules. Further structural idealisation and restrained refinement was carried out using *REFMAC*5 [68]. Initial phases for Mth373_NX were determined by the molecular replacement program *MolRep* [69] and the refined crystal structure of Mth373_NU. X-ray diffraction data and final refinement statistics are listed in Table 1. Structural coordinates and structure factors for Mth373_NU and Mth373_NX have been deposited in the RCSB PDB under accession codes PDB: 8W3U and PDB: **9AR1**, respectively. Attempts to produce crystal structures of additional *M. thermautotrophicus* enzymes Mth1789, Mth631 and Mth380 failed to produce crystals of sufficient quality for crystal structure determination.

Molecular modelling

Structural homologues of Mth375 were identified utilising the online structural alignment server CLICK [37]. The detection of similarities in structural subdomains enabled the deeper inspection of NS-SDR active sites accounting for their potential induced fit plasticity when UDP-sugar substrates are bound. The selected structures (Table 2) with varying activities or bound substrate were submitted to SALIGN [72] and the resultant structure-based sequence alignments were visualised utilising Clustal Omega (0.1.2.4) multiple sequence alignment online server [38]. *In silico* models of *M. thermautotrophicus* enzymes Mth1789, Mth631 and Mth380 were developed using the ICM-Homology modelling algorithm, utilising the full refinement of side chains and loops option available in the ICM-Pro modelling suite (Molsoft LLC; www.molsoft.com) [50,51]. ICM-Pro was also used for template searches for our candidate proteins, allowing for automated alignment and inspection prior to modelling the target proteins, including associated cofactors and substrates where possible. Protein identities and template details are shown in Table 4. The resultant models of Mth1789, Mth631 and Mth380, and the crystal structures of Mth375_NU (PDB: 6PNL) and Mth373_NX (PDB: 9AR1) were superimposed using SALIGN [72] and aligned sequences visualised using Clustal Omega (0.1.2.4) multiple sequence alignment online server [38] (see Table 4). Molecular docking experiments were carried out on the crystal structure of Mth375 (PDB: 6PNL) using the program GOLD (Genetic Optimization for Ligand Docking) version 5.2 favouring the GOLD Scoring system [39]. The search domain was centred on the terminal phosphate of the bound UDP molecule with radius set to 15 Å and executed using a 100% search efficiency, generating 10 Genetic Algorithm (GA) runs. A scaffold-based constraint was also employed so that docked compounds mimicked the bond overlap observed in the bound UDP molecule. All library definitions for the rotameric state of residues Asn91, Ser129, Cys131, Tyr155, Asn184, Asn197, Thr215, Arg281 and Trp283 were allowed during the docking run. The generated binding poses of potential substrates were inspected, and conformations were chosen for further analysis taking into account their ranking and interactions with active site residues. The structural context for sequence conservation was analysed using the ConSurf server [73].

Phylogenetic analysis of hexose epimerase sequences

The epimerase amino acid sequences in a previously published phylogenetic analysis [36] together with sequences for methanogen and homologous protein crystal structures were downloaded from the nonredundant NCBI or RCSB databases and imported into MEGA7. The sequences were aligned using Clustal and a Neighbour-Joining phylogenetic tree [74] constructed in MEGA7 using default parameter settings [75].

Acknowledgements

We would like to acknowledge the generous support of the Marsden Fund through the Royal Society of New Zealand (AGR1301). We would also like to acknowledge the help from the Pastoral Greenhouse Gas Research Consortium for the support of Denise Schäfer for her bachelor thesis internship. We thank Debjit Dey for the growth of *Methanothermobacter thermautotrophicus* ΔH and DNA isolation. We thank Don Otter

and Bryan Treloar for helping with aminosugar gas chromatography analyses. We also greatly appreciate the support from the Australian Synchrotron and the New Zealand Synchrotron Group. This research was undertaken on the MX1 and MX2 beamlines at the Australian Synchrotron, part of ANSTO (Australian Nuclear Science and Technology Organisation), and made use of the Australian Cancer Research Foundation (ACRF) detector. Open access publishing facilitated by AgResearch Ltd, as part of the Wiley - AgResearch Ltd agreement via the Council of Australian University Librarians.

Conflict of interest

The authors declare that they have no conflicts of interest with the contents of this article.

Author contributions

RR conceptualisation; RR, LS, VC, PE and AS-S methodology; VC data collection, curation and formal analysis; RR, VC, LS and AS-S writing and review; VC visualisations; R.R. supervision, project administration and funding acquisition.

Data availability statement

The data supporting the findings of this study can be found within the article. Structural coordinates and structure factors can be found in the RCSB, with PDB codes 6PNL (https://www.rcsb.org/structure/6PNL), 6PMH (https://www.rcsb.org/structure/6PMH), 9AR1 (https://www.rcsb.org/structure/9AR1) and 8W3U (https://www.rcsb.org/structure/8W3U).

References

1 Errington J (2013) L-form bacteria, cell walls and the origins of life. *Open Biol* **3**, 120143.
2 Albers SV & Meyer BH (2011) The archaeal cell envelope. *Nat Rev Microbiol* **9**, 414–426.
3 Smith CA (2006) Structure, function and dynamics in the *mur* family of bacterial cell wall ligases. *J Mol Biol* **362**, 640–655.
4 Scheffers DJ & Pinho MG (2005) Bacterial cell wall synthesis: new insights from localization studies. *Microbiol Mol Biol Rev* **69**, 585–607.
5 Bouhss A, Trunkfield AE, Bugg TD & Mengin-Lecreulx D (2008) The biosynthesis of peptidoglycan lipid-linked intermediates. *FEMS Microbiol Rev* **32**, 208–233.
6 El Zoeiby A, Sanschagrin F & Levesque RC (2003) Structure and function of the Mur enzymes: development of novel inhibitors. *Mol Microbiol* **47**, 1–12.
7 Sauvage E, Kerff F, Terrak M, Ayala JA & Charlier P (2008) The penicillin-binding proteins: structure and role in peptidoglycan biosynthesis. *FEMS Microbiol Rev* **32**, 234–258.
8 Halliday J, McKeveney D, Muldoon C, Rajaratnam P & Meutermans W (2006) Targeting the forgotten transglycosylases. *Biochem Pharmacol* **71**, 957–967.
9 Ellen AF, Zolghadr B, Driessen AM & Albers SV (2010) Shaping the archaeal cell envelope. *Archaea* **2010**, 608243.
10 Kandler O & König H (1993) In Cell Envelopes of Archaea: Structure and Chemistry in the Biochemistry of Archaea (Archaebacteria) (Kates M, Kushner DJ & Matheson AT, eds), pp. 223–259. Elsevier, Amsterdam, the Netherlands.
11 Kandler O & König H (1998) Cell wall polymers in archaea (archaebacteria). *Cell Mol Life Sci* **54**, 305–308.
12 Kandler O (1994) Cell wall biochemistry and three-domain concept of life. *Syst Appl Microbiol* **16**, 501–509.
13 Rachel R (2010) Cell envelopes of Crenarchaeota and Nanoarchaeota. In Prokaryotic Cell Wall Compounds: Structure and Biochemistry (König H, Claus H & Varma A, eds), pp. 271–291. Springer Berlin Heidelberg, Berlin, Heidelberg.
14 Lupo V, Roomans C, Royen E, Ongena L, Jacquemin O, Kerff F & Baurain D (2022) Origin and evolution of pseudomurein biosynthetic gene clusters. *bioRxiv*. doi: 10.1101/2022.11.30.518518
15 König H, Kandler O & Hammes W (1989) Biosynthesis of pseudomurein: isolation of putative precursors from *Methanobacterium thermoautotrophicum*. *Can J Microbiol* **35**, 176–181.
16 Hartmann E & König H (1990) Comparison of the biosynthesis of the methanobacterial pseudomurein and the eubacterial murein. *Naturwissenschaften* **77**, 472–475.
17 Claus H & König H (2010) Cell envelopes of methanogens. In Prokaryotic Cell Wall Compounds: Structure and Biochemistry (König H, Claus H & Varma A, eds), pp. 231–251. Springer, Berlin.
18 König H & Kandler O (1979) *N*-Acetyltalosaminuronic acid a constituent of the pseudomurein of the genus *Methanobacterium*. *Arch Microbiol* **123**, 295–299.
19 König H & Kandler O (1980) 2-amino-2-deoxytaluronic acid and 2-amino-2-deoxyglucose from the pseudomurein of *Methanobacterium thermoautotrophicum* possess the L- and D-configurations, respectively. *Hoppe Seylers Z Physiol Chem* **361**, 981–983.
20 Subedi BP, Martin WF, Carbone V, Duin EC, Cronin B, Sauter J, Schofield LR, Sutherland-Smith AJ & Ronimus RS (2021) Archaeal pseudomurein and bacterial murein cell wall biosynthesis share a common evolutionary ancestry. *FEMS Microbes* **2**, xtab012.

21 Subedi BP, Schofield LR, Carbone V, Wolf M, Martin WF, Ronimus RS & Sutherland-Smith AJ (2022) Structural characterisation of methanogen pseudomurein cell wall peptide ligases homologous to bacterial MurE/F murein peptide ligases. *Microbiology* **168**, 001235.
22 Kanehisa M, Sato Y, Kawashima M, Furumichi M & Tanabe M (2016) KEGG as a reference resource for gene and protein annotation. *Nucleic Acids Res* **44**, D457–D462.
23 van Heijenoort J (1998) Assembly of the monomer unit of bacterial peptidoglycan. *Cell Mol Life Sci* **54**, 300–304.
24 Allard ST, Giraud MF & Naismith JH (2001) Epimerases: structure, function and mechanism. *Cell Mol Life Sci* **58**, 1650–1665.
25 Namboori SC & Graham DE (2008) Acetamido sugar biosynthesis in the Euryarchaea. *J Bacteriol* **190**, 2987–2996.
26 Carbone V, Schofield LR, Sang C, Sutherland-Smith AJ & Ronimus RS (2018) Structural determination of archaeal UDP-*N*-acetylglucosamine 4-epimerase from *Methanobrevibacter ruminantium* M1 in complex with the bacterial cell wall intermediate UDP-*N*-acetylmuramic acid. *Proteins* **86**, 1306–1312.
27 Van Overtveldt S, Verhaeghe T, Joosten HJ, van den Bergh T, Beerens K & Desmet T (2015) A structural classification of carbohydrate epimerases: from mechanistic insights to practical applications. *Biotechnol Adv* **33**, 1814–1828.
28 Smith DR, Doucette-Stamm LA, Deloughery C, Lee H, Dubois J, Aldredge T, Bashirzadeh R, Blakely D, Cook R, Gilbert K *et al.* (1997) Complete genome sequence of *Methanobacterium thermoautotrophicum* ΔH: functional analysis and comparative genomics. *J Bacteriol* **179**, 7135–7155.
29 Islam R, Brown S, Taheri A & Dumenyo CK (2019) The gene encoding NAD-dependent epimerase/dehydratase, *wcaG*, affects cell surface properties, virulence, and extracellular enzyme production in the soft rot phytopathogen, *Pectobacterium carotovorum*. *Microorganisms* **7**, 172.
30 McCallum M, Shaw GS & Creuzenet C (2011) Characterization of the dehydratase WcbK and the reductase WcaG involved in GDP-6-deoxy-*manno*-heptose biosynthesis in *Campylobacter jejuni*. *Biochem J* **439**, 235–248.
31 Kavanagh KL, Jornvall H, Persson B & Oppermann U (2008) The SDR superfamily: functional and structural diversity within a family of metabolic and regulatory enzymes. *Cell Mol Life Sci* **65**, 3895–3906.
32 Persson B & Kallberg Y (2013) Classification and nomenclature of the superfamily of short-chain dehydrogenases/reductases (SDRs). *Chem Biol Interact* **202**, 111–115.
33 Sakuraba H, Kawai T, Yoneda K & Ohshima T (2011) Crystal structure of UDP-galactose 4-epimerase from the hyperthermophilic archaeon *Pyrobaculum calidifontis*. *Arch Biochem Biophys* **512**, 126–134.
34 King JD, Harmer NJ, Preston A, Palmer CM, Rejzek M, Field RA, Blundell TL & Maskell DJ (2007) Predicting protein function from structure – the roles of short-chain dehydrogenase/reductase enzymes in *Bordetella* O-antigen biosynthesis. *J Mol Biol* **374**, 749–763.
35 Krissinel E & Henrick K (2007) Inference of macromolecular assemblies from crystalline state. *J Mol Biol* **372**, 774–797.
36 Ishiyama N, Creuzenet C, Lam JS & Berghuis AM (2004) Crystal structure of WbpP, a genuine UDP-*N*-acetylglucosamine 4-epimerase from *Pseudomonas aeruginosa*: substrate specificity in UDP-hexose 4-epimerases. *J Biol Chem* **279**, 22635–22642.
37 Nguyen MN, Tan KP & Madhusudhan MS (2011) CLICK – topology-independent comparison of biomolecular 3D structures. *Nucleic Acids Res* **39**, W24–W28.
38 Sievers F, Wilm A, Dineen D, Gibson TJ, Karplus K, Li W, Lopez R, McWilliam H, Remmert M, Soding J *et al.* (2011) Fast, scalable generation of high-quality protein multiple sequence alignments using Clustal omega. *Mol Syst Biol* **7**, 539.
39 Verdonk ML, Cole JC, Hartshorn MJ, Murray CW & Taylor RD (2003) Improved protein-ligand docking using GOLD. *Proteins* **52**, 609–623.
40 Weik M, Ravelli RB, Kryger G, McSweeney S, Raves ML, Harel M, Gros P, Silman I, Kroon J & Sussman JL (2000) Specific chemical and structural damage to proteins produced by synchrotron radiation. *Proc Natl Acad Sci U S A* **97**, 623–628.
41 Langer G, Cohen SX, Lamzin VS & Perrakis A (2008) Automated macromolecular model building for X-ray crystallography using ARP/wARP version 7. *Nat Protoc* **3**, 1171–1179.
42 Yin B, Cui D, Zhang L, Jiang S, Machida S, Yuan YA & Wei D (2014) Structural insights into substrate and coenzyme preference by SDR family protein Gox2253 from *Gluconobater oxydans*. *Proteins* **82**, 2925–2935.
43 Polizzi SJ, Walsh RM Jr, Peeples WB, Lim J-M, Wells L & Wood ZA (2012) Human UDP-α-D-xylose synthase and *Escherichia coli* ArnA conserve a conformational shunt that controls whether xylose or 4-keto-xylose is produced. *Biochemistry* **51**, 8844–8855.
44 Savino S, Borg AJE, Dennig A, Pfeiffer M, de Giorgi F, Weber H, Dubey KD, Rovira C, Mattevi A & Nidetzky B (2019) Deciphering the enzymatic mechanism of sugar ring contraction in UDP-apiose biosynthesis. *Nature Catalysis* **2**, 1115–1123.
45 Williams GJ, Breazeale SD, Raetz CR & Naismith JH (2005) Structure and function of both domains of

ArnA, a dual function decarboxylase and a formyltransferase, involved in 4-amino-4-deoxy-L-arabinose biosynthesis. *J Biol Chem* **280**, 23000–23008.
46 Schulz JM, Watson AL, Sanders R, Ross KL, Thoden JB, Holden HM & Fridovich-Keil JL (2004) Determinants of function and substrate specificity in human UDP-galactose 4′-epimerase. *J Biol Chem* **279**, 32796–32803.
47 Thoden JB, Henderson JM, Fridovich-Keil JL & Holden HM (2002) Structural analysis of the Y299C mutant of *Escherichia coli* UDP-galactose 4-epimerase. Teaching an old dog new tricks. *J Biol Chem* **277**, 27528–27534.
48 Guo H, Li L & Wang PG (2006) Biochemical characterization of UDP-GlcNAc/Glc 4-epimerase from *Escherichia coli* O86:B7. *Biochemistry* **45**, 13760–13768.
49 Shin SM, Choi JM, di Luccio E, Lee YJ, Lee SJ, Lee SH & Lee DW (2015) The structural basis of substrate promiscuity in UDP-hexose 4-epimerase from the hyperthermophilic eubacterium *Thermotoga maritima*. *Arch Biochem Biophys* **585**, 39–51.
50 Abagyan R, Batalov S, Cardozo T, Totrov M, Webber J & Zhou Y (1997) Homology modeling with internal coordinate mechanics: deformation zone mapping and improvements of models via conformational search. *Proteins* **1**, 29–37.
51 Cardozo T, Totrov M & Abagyan R (1995) Homology modeling by the ICM method. *Proteins* **23**, 403–414.
52 Da Costa M, Gevaert O, Van Overtveldt S, Lange J, Joosten HJ, Desmet T & Beerens K (2021) Structure-function relationships in NDP-sugar active SDR enzymes: fingerprints for functional annotation and enzyme engineering. *Biotechnol Adv* **48**, 107705.
53 Allard ST, Cleland WW & Holden HM (2004) High resolution X-ray structure of dTDP-glucose 4,6-dehydratase from *Streptomyces venezuelae*. *J Biol Chem* **279**, 2211–2220.
54 Somers WS, Stahl ML & Sullivan FX (1998) GDP-fucose synthetase from *Escherichia coli*: structure of a unique member of the short-chain dehydrogenase/reductase family that catalyzes two distinct reactions at the same active site. *Structure* **6**, 1601–1612.
55 Menon S, Stahl M, Kumar R, Xu GY & Sullivan F (1999) Stereochemical course and steady state mechanism of the reaction catalyzed by the GDP-fucose synthetase from *Escherichia coli*. *J Biol Chem* **274**, 26743–26750.
56 Chang S, Duerr B & Serif G (1988) An epimerase-reductase in L-fucose synthesis. *J Biol Chem* **263**, 1693–1697.
57 Wedlock DN, Pedersen G, Denis M, Dey D, Janssen PH & Buddle BM (2010) Development of a vaccine to mitigate greenhouse gas emissions in agriculture: vaccination of sheep with methanogen fractions induces antibodies that block methane production *in vitro*. *N Z Vet J* **58**, 29–36.
58 Wooh JW, Kidd RD, Martin JL & Kobe B (2003) Comparison of three commercial sparse-matrix crystallization screens. *Acta Crystallogr D Biol Crystallogr* **59**, 769–772.
59 Fazio VJ, Peat TS & Newman J (2014) A drunken search in crystallization space. *Acta Crystallogr F Struct Biol Commun* **70**, 1303–1311.
60 Aragao D, Aishima J, Cherukuvada H, Clarken R, Clift M, Cowieson NP, Ericsson DJ, Gee CL, Macedo S, Mudie N *et al.* (2018) MX2: a high-flux undulator microfocus beamline serving both the chemical and macromolecular crystallography communities at the Australian Synchrotron. *J Synchrotron Radiat* **25**, 885–891.
61 Cowieson NP, Aragao D, Clift M, Ericsson DJ, Gee C, Harrop SJ, Mudie N, Panjikar S, Price JR, Riboldi-Tunnicliffe A *et al.* (2015) MX1: a bending-magnet crystallography beamline serving both chemical and macromolecular crystallography communities at the Australian Synchrotron. *J Synchrotron Radiat* **22**, 187–190.
62 McPhillips TM, McPhillips SE, Chiu HJ, Cohen AE, Deacon AM, Ellis PJ, Garman E, Gonzalez A, Sauter NK, Phizackerley RP *et al.* (2002) *Blu-ice* and the *distributed control system*: software for data acquisition and instrument control at macromolecular crystallography beamlines. *J Synchrotron Radiat* **9**, 401–406.
63 Kabsch W (2010) Integration, scaling, space-group assignment and post-refinement. *Acta Crystallogr D Biol Crystallogr* **66**, 133–144.
64 Evans P (2006) Scaling and assessment of data quality. *Acta Crystallogr D Biol Crystallogr* **62**, 72–82.
65 McCoy AJ, Grosse-Kunstleve RW, Adams PD, Winn MD, Storoni LC & Read RJ (2007) *Phaser* crystallographic software. *J Appl Cryst* **40**, 658–674.
66 Winn MD, Ballard CC, Cowtan KD, Dodson EJ, Emsley P, Evans PR, Keegan RM, Krissinel EB, Leslie AG, McCoy A *et al.* (2011) Overview of the *CCP*4 suite and current developments. *Acta Crystallogr D Biol Crystallogr* **67**, 235–242.
67 Emsley P, Lohkamp B, Scott WG & Cowtan K (2010) Features and development of *coot*. *Acta Crystallogr D Biol Crystallogr* **66**, 486–501.
68 Murshudov GN, Skubák P, Lebedev AA, Pannu NS, Steiner RA, Nicholls RA, Winn MD, Long F & Vagin AA (2011) *REFMAC*5 for the refinement of macromolecular crystal structures. *Acta Crystallogr D Biol Crystallogr* **67**, 355–367.
69 Vagin A & Teplyakov A (1997) *MOLREP*: an automated program for molecular replacement. *J Appl Cryst* **30**, 1022–1025.
70 Long F, Vagin AA, Young P & Murshudov GN (2008) *BALBES*: a molecular-replacement pipeline. *Acta Crystallogr D Biol Crystallogr* **64**, 125–132.

71 Allard ST, Beis K, Giraud MF, Hegeman AD, Gross JW, Wilmouth RC, Whitfield C, Graninger M, Messner P, Allen AG *et al*. (2002) Toward a structural understanding of the dehydratase mechanism. *Structure* **10**, 81–92.
72 Braberg H, Webb BM, Tjioe E, Pieper U, Sali A & Madhusudhan MS (2012) SALIGN: a web server for alignment of multiple protein sequences and structures. *Bioinformatics* **28**, 2072–2073.
73 Yariv B, Yariv E, Kessel A, Masrati G, Chorin AB, Martz E, Mayrose I, Pupko T & Ben-Tal N (2023) Using evolutionary data to make sense of macromolecules with a "face-lifted" ConSurf. *Protein Sci* **32**, e4582.
74 Saitou N & Nei M (1987) The neighbor-joining method: a new method for reconstructing phylogenetic trees. *Mol Biol Evol* **4**, 406–425.
75 Kumar S, Stecher G & Tamura K (2016) MEGA7: molecular evolutionary genetics analysis version 7.0 for bigger datasets. *Mol Biol Evol* **33**, 1870–1874.
76 Beerens K, Soetaert W & Desmet T (2015) UDP-hexose 4-epimerases: a view on structure, mechanism and substrate specificity. *Carbohydr Res* **414**, 8–14.
77 Schofield LR, Beattie AK, Tootill CM, Dey D & Ronimus RS (2015) Biochemical characterisation of phage pseudomurein endoisopeptidases PeiW and PeiP using synthetic peptides. *Archaea* **2015**, 828693.
78 Z E & P L (1965) Evolutionary divergence and convergence in proteins. In Evolving Genes and Proteins (Vernon B & Henry JV, eds), pp. 97–166. Academic Press, New York, NY, USA.